2014-08-26

Investigating the effect of proteoglycan 4 on hyaluronan solution properties using confocal fluorescence recovery after photobleachin

Bloom, Adam

UNIVERSITY OF CALGARY

Investigating the effect of proteoglycan 4 on hyaluronan solution properties using confocal fluorescence recovery after photobleaching

by

Adam Kennedy Bloom

A THESIS

SUBMITTED TO THE FACULTY OF GRADUATE STUDIES

IN PARTIAL FULFILMENT OF THE REQUIREMENTS FOR THE

DEGREE OF MASTER OF SCIENCE

GRADUATE PROGRAM IN BIOMEDICAL ENGINEERING

CALGARY, ALBERTA

AUGUST, 2014

Abstract

Hyaluronan (HA) and proteoglycan 4 (PRG4) are vital macromolecular constituents of synovial fluid (SF) that contribute synergistically to its biophysical properties.

The objective of this thesis was to use confocal fluorescence recovery after photobleaching (FRAP) to determine whether PRG4 will decrease the permeability of simple HA solutions due to specific interactions between PRG4 and HA polymers in solution.

Bovine and recombinant human PRG4 caused HA solutions of all concentrations to become less permeable to tracer molecules. This effect, specific to PRG4 and not seen with a control protein, was not dependent on protein structure as determined by reducing and alkylating PRG4. Additionally, confocal FRAP was successfully employed to study human SF samples of interest.

These results demonstrate PRG4 can alter solution properties of HA, possibly due to entanglement through binding and/or HA crowding PRG4 into a self-assembled network. These results contribute to the understanding of PRG4's role in SF.

Preface

The following thesis is presented in a partial manuscript based format, and therefore there is some repetition between chapters in regards to the introductions and methods sections. Chapter 1 is an introduction that provides relevant background information. Chapter 2 is in preparation for submission*;*

Bloom AK, Samsom ML, Steele BL, Schmidt TA. Investigating the effect of proteoglycan 4 on hyaluronan solution properties using confocal fluorescence recovery after photobleaching. Biorheology.

As such, Chapter 2 is intended to be a standalone study, while Chapters 3 and 4 build upon the findings of Chapter 2. Chapter 5 is a summary of findings, followed by references in Chapter 6.

Acknowledgements

- I would like to thank my supervisor Dr. Tannin Schmidt for the opportunity and for giving me guidance through my research while supporting my future goals and dreams. I would also like to thank him for creating a positive, friendly and supportive work environment within the lab.

- I would like to thank Dr. Kristina Rinker, and Dr. Neil Duncan for serving on my supervisory committee, and providing guidance and insightful questions towards my research.

- I would like to thank my past and present lab mates: Bridgett, Bryan, Mike, Saleem, Sam, Suresh, and Taryn for the generous amount of help each has given. I would like to especially thank Bridgett for teaching me how to use the confocal microscope, Michael for his role in developing the Matlab® analysis code, and Taryn for her characterization of SF samples.

- I would like to thank my parents Ira and Carol for all they do to make life easier in my early 20's.

- Lastly I would like to thank my friends, especially the ones who stand by me unconditionally and are comfortable to just hang out and do nothing. You are my route to happiness and what makes it all worth it.

Table of Contents

List of Tables

List of Figures and Illustrations

List of Symbols, Abbreviations and Nomenclature

Symbol	Definition
[HA]	Hyaluronan concentration
[PRG4]	Proteoglycan 4 concentration
$<\mu_{kinetic}, Neq>$	Static coefficient of friction calculated using equilibrium load
β	Empirical constant for universal scaling equation
γ	Empirical constant for universal scaling equation
λ_n	n^{th} root of J_0
$\mu_{(2,i)}$	Second central moment
ξ	Apparent Mesh Size Distribution
ω	half width of the e^{-2} value of the Gaussian
ANOVA	Analysis of variance
BCA	Bicinchoninic acid assay
BSA	Bovine serum albumin
CACP	Camptodactyl-arthropathy-coxavara-pericarditis
CHO	Chinese hamster ovary cells
C_n	Defined in Equation 2 (section 1.3.2)
d	Hydrodynamic diameter of tracer
D_t	Lateral diffusion coefficient
D_t^0	Free lateral diffusion coefficient in PBS
DEAE	Diethylaminoethyl
ELISA	Enzyme-Linked Immunosorbent Assay
EMSA	Electrophoretic mobility shift assay
F(0)	Fluorescent intensity at immediately after bleaching
$F(\infty)$	Final equilibrium fluorescent intensity after bleaching
f(r)	Initial condition for calculating C_n
F_0	Initial pre-bleach fluorescent intensity
FITC	Fluorescein isothiocyanate
FRAP	Fluorescence Recovery After Photobleaching
HA	Hyaluronan
I	Fluorescent intensity
I_1	Coefficient for Equation 1
IE	Fluorescent intensity at immediately after bleaching
J_n	nth order Bessel function
K	Immobile fraction
LPN	Anti-PRG4 antibody, C-terminal
MPTM	Multiple Particle Tracking Micro-rheology
MW	Molecular Weight
NA	Numerical Aperature

NR	Non-Reduced
NSAID	Non-Steroidal Anti-Inflammatory
OA	Osteoarthritis
PBS	Phosphate buffered saline
PEX	Hemopexin
PNA	Peanut agglutinin
PRG4	Proteoglycan 4
r	Radius
R	Total radius of bleached area
R/A	Reduced and alkylated
rhPRG4	Recombinant human PRG4
SDS-PAGE	Sodium Dodecyl Sulfate Polyacrylamide Gel Electrophoresis
SEM	Standard error of the mean
SMB	Somatomedin B
STD	Standard deviation
t	Time
T_1	Characteristic Time (Equation 1)
TJR	Total joint replacement

CHAPTER 1: INTRODUCTION

1.1 SYNOVIAL FLUID OVERVIEW

1.1.1 SYNOVIAL JOINTS AND SYNOVIAL FLUID

Synovial fluid (SF) is a viscous non-Newtonian fluid, which takes its namesake from its similar consistency to egg yolk. SF is found within diarthrodial joints, more commonly known as synovial joints. All synovial joints contain the same essential structures (**Figure 1-1**).

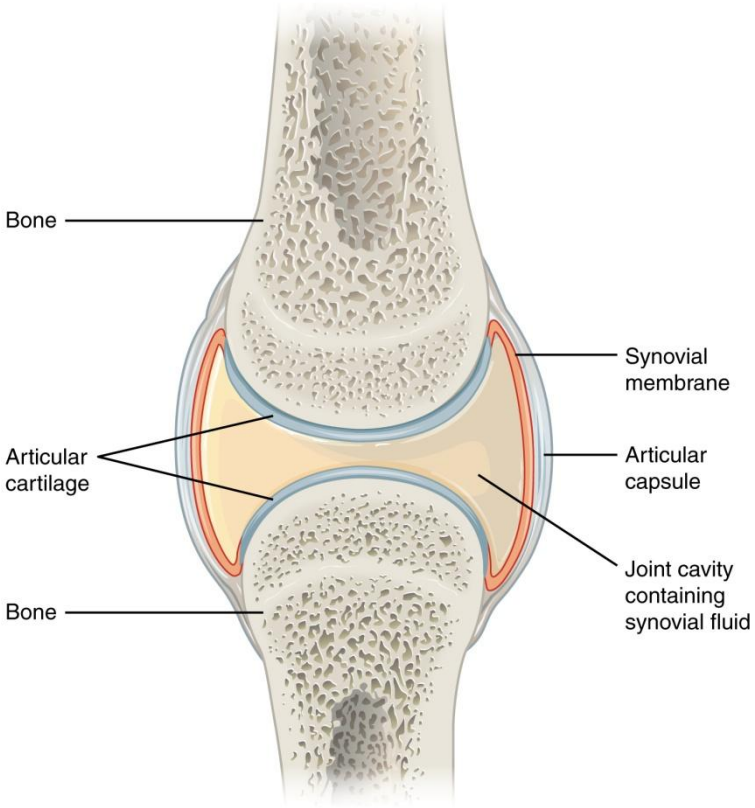

Figure 1-1: A schematic of the diarthrodial joint [1].

These joints contain two articulating bones which have their contacting ends covered with articulating cartilage making a smooth slippery surface. The articulating ends of the bones are connected by an articular capsule. This capsule contains an outer fibrous membrane and ligaments which hold the bones together, and an inner synovial membrane which secretes SF between the articulating bones. SF is essential to lubrication, shock absorption, as well as nourishing and immune properties[2]. Two important lubricating components of SF are the macromolecules proteoglycan 4 (PRG4) and hyaluronan (HA). PRG4 is a boundary lubricant which coats the cartilage surface, while HA supplies viscoelasticity in addition to its lubricating ability. These macromolecules will be discussed in detail within Section 1.2 of this chapter.

1.1.2 SYNOVIAL FLUID LUBRICATION

Synovial joints are able to generate extremely low coefficients of friction in comparison to mechanical systems[3]. Many theories have been presented to explain how this extremely effective lubrication works within biological systems. It is inherent that the lubricating properties of articular cartilage are a function of the material properties of the tissue, the biophysical properties of surface macromolecules, and interaction with SF[4]. It's also plausible that joint lubrication is the product of multiple mechanisms and the dominant mechanism of lubrication is dependent on variables such as: contact pressure, duration of loading and molecular components at the surface membrane[4].

Lubrication of the articular joints by SF may occur in a variety of regimes, classically defined as boundary lubrication, mixed lubrication, and hydrodynamic lubrication[5]. These three regimes are illustrated in **Figure 1-2**, which is commonly referred to as a Stribeck Curve.

The Stribeck curve was generated by measuring the lubrication of steel surfaces in engines, and therefore represents an idealized system in comparison to porous hydrogels such as the cartilage on cartilage interface within synovial joints.

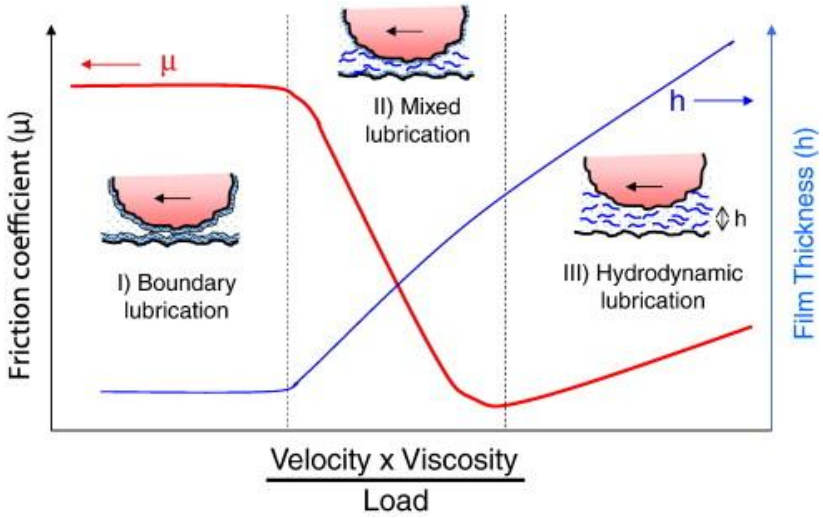

Figure 1-2: Schematic of boundary, mixed and film lubrication[5].

In hydrodynamic lubrication the articular cartilage surfaces are separated by a fluid film, which usually occurs in cases of low joint loads and high solution viscosity. Theories which stress the importance of a fluid film may have some validity, but the case of a load bearing joint such as the knee rejects the fluid film as an essential quality of synovial joints. Specifically, an article by Calgaris and Ateshian[6] demonstrates how under an applied load fluid will drain out of the joint decreasing the importance of fluid film lubrication.

Boundary lubrication is a specific mode of lubrication where surface to surface contact between cartilage surfaces occurs, and a thin film of macromolecules coating and separating the surfaces is responsible for lubrication. Boundary lubrication occurs under high joint loads and slow speeds, causing the articular cartilage surfaces to squeeze together. To function as a boundary lubricant a macromolecule must adhere to the surface of the articular cartilage,

changing the physiochemical nature of the surface, and cause the two surfaces to repel each other[7]. Mixed lubrication is simply the combination of boundary and hydrodynamic lubrication, occurring when some contact between surfaces and some fluid film separation is present.

The macromolecules PRG4 and HA are essential to both boundary lubrication as well as maintaining the high viscosity responsible for fluid film lubrication [8]. These concepts will be expanded on in Section 1.2.

1.1.3 SYNOVIAL FLUID VISCOELASTIC BEHAVIOUR

An important quality of synovial joints, such as the knee, is their ability to dampen and withstand high impact loads sustained while running or jumping[9]. While the majority of this ability stems from the structure of articular cartilage and subchondral bone, SF also aids in the dissipation of high energy impacts to synovial joints through the fluids mechanical behaviour [2]. The high molecular weight HA polymer content of SF results in a highly viscous solution. The HA polymers overlap and entangle within solution to create a polymer network with elastic and shear thinning properties[10]. While the majority of SF rheology and elastic behaviour is resultant from HA, some studies have indicated that proteins within SF can aggregate and contribute to some of the rheological behaviour of SF[11]. The structure and physiology of HA will be expanded upon in Section 1.2.

The dynamic rigidity of SF, or ratio of the peak stress to peak strain, can be divided into two components: the dynamic loss module and the elastic module of SF; the former representing the amount of energy lost to heat and the later representing energy stored when the solution is

subjected to strain. At low frequency strain, the dynamic loss module is typically higher than the elastic module for SF, indicating little energy is stored by the elastic nature of the system. However, as the frequency of strain increases the elastic module increases and surpasses the dynamic loss module. This suggests that at low frequency strain SF acts as a viscous fluid, and at high frequency strain SF acts elastically to store the energy. On the molecular scale, this can be interpreted such that the configuration of the polymers is able to change at low frequency strain and the polymers cannot slip past each other, but at high frequency the molecules are unable to adjust or manipulate there configuration so molecules interlock and the energy is contained mechanically within the system. This rapid and reversible change from viscous solution to elastic polymer solution is a significant aspect of SF physiology[10].

1.1.4 SYNOVIAL FLUID NOURISHING AND IMMUNE FUNCTIONS

In addition to SF lubrication and elastic behaviour, SF provides a variety of functions within the synovial joint. SF is a complex mixture of blood proteins, immune cells, cytokines, etc., and works to keep the synovium and articular cartilage nourished and healthy. The polymer matrix within SF is important because it provides a support matrix for cells, and filters out large particles without hindering the transport of small particles such as oxygen and nutritional compounds [12]. This, in combination with SF other functions, stresses that the three dimensional network of SF is important to a variety of SF functions and physiology.

1.1.5 OSTEOARTHRITIS AND SYNOVIAL FLUID

Osteoarthritis (OA) is a disease involving the chronic breakdown of cartilage which effects over 3 million Canadians[13]. The disease is characterized by symptoms of swelling, pain and joint stiffness. OA typically affects older patients, and continues to worsen with age, which places an increasingly heavy burden on the health care system as a large proportion of our population becomes elderly. Currently OA is treated with therapeutic exercise, pain medication (analgesics and NSAID) and total joint replacement surgery[13]. Due to the limited lifespan of artificial joints, total joint replacement is an unacceptable treatment to younger patients and there is a growing demand for more sustainable and less invasive treatment methods.

Significant variation in the composition of SF has been found within a certain sub population of OA patients, which questions the role of SF and joint lubrication in OA's characteristic breakdown of cartilage. It has been shown in studies that many SF samples of OA patients contain low levels of PRG4, and HA with reduced molecular weight (MW)[14]. This change in SF was then shown to decrease the lubricating ability of the SF possibly contributing to the eventual cartilage damage in the patients[14]. This reduction of PRG4 concentration in SF has also been shown in multiple OA animal models[15-17].

While the previously mentioned studies have shown PRG4 concentration and HA MW to decrease in OA patients, there are numerous other studies that have the opposite findings. For example in some studies PRG4 concentration is shown to increase in late stage OA, or after intra-articular fracture[18, 19]. Therefore it is important to stress that the alteration of SF chemistry, and ensuing change in physiology, is a complex problem. It is however possible to address the mechanisms of disease and potential treatment of OA patients who fall under certain

sub populations. The next section of this introductory chapter will attend to PRG4 and HA biochemistry and function in detail, to better understand SF and begin to address gaps in our understanding. An advanced understanding of SF physiology will hopefully enable more effective treatments to OA and joint disease as a whole.

1.2 SYNOVIAL FLUID CONSTITUENTS

1.2.1 HYALURONAN

HA is a major component of SF and its major role is to impart fluid viscosity and elasticity which helps lubricate and transfer loads across cartilage within articulating joint[20]. HA is a negatively charged biopolymer composed of alternating D-glucuronic acid and N-acetylglucosamine[21]. The molecule has an average molecular mass of 4MDa and is typically found at concentrations of 1-4mg/ml in synovial fluid[2]. HA takes a rigid left handed helical shape in aqueous solution and has been shown to take extended and condensed conformations under a variety of different environmental conditions[22]. Under low concentrations, HA occupies large hydrodynamic volumes and takes a semi flexible random coil conformation[22]. As the concentration of HA approaches and passes the critical concentration for domain overlap, the macromolecule accommodates to its neighbouring molecules by compacting and reducing domain sizes[22]. HA of all conformations have been shown to create networks and large twisted fibers[22]. The solution network of HA within SF can be thought of as a dense entanglement of semi-flexible polymers[22]. Each individual molecule takes up a large amount of space, typically modeled as a sphere, which effectively crowds other macromolecules[22]. This crowding reduces the volume available to other molecules in the system, and has many physiological implications including an increase in the effective concentration and promoting the formation of

multimer species among other macromolecules occupying the solution [23, 24]. HA is capable of varying its shape and conformations while adhering to surfaces, depending on the type of surface and relevant interactions with the surface[25].

There is a discrepancy for whether or not HA functions as a cartilage boundary lubricant which is most likely due to the variance of experimental test surfaces and configurations[8]. It is also likely that this discrepancy is due to a complex mechanism of boundary lubrication from HA that has yet to be elucidated[26]. In some studies, HA is shown to have no lubricating effect in absence of other proteinaceous SF constituents[27]. A study by Chan, et al. shows that HA only marginally lubricates the cartilage surface when tested using an atomic force microscope[28]. In contrast to these studies, many experiments have shown that HA does in fact have a boundary lubricating function[14, 29]. In a study by Schmidt, et al. [8], HA was shown to reduce the kinetic coefficient of friction ($\mu_{kinetic,\ Neq}$) between two sliding cartilage samples under a stationary area of contact from 0.24 using phosphate buffered saline(PBS) to 0.12 when lubricating with 3,300µg/ml HA. **Figure 1-3** shows a summary of HA boundary lubricating ability as a function of concentration compared to PBS. Additionally, a lower distribution of HA MW has been shown to significantly, but slightly, decrease HA's lubricating ability on articular cartilage (**Figure 1-4**)[30].

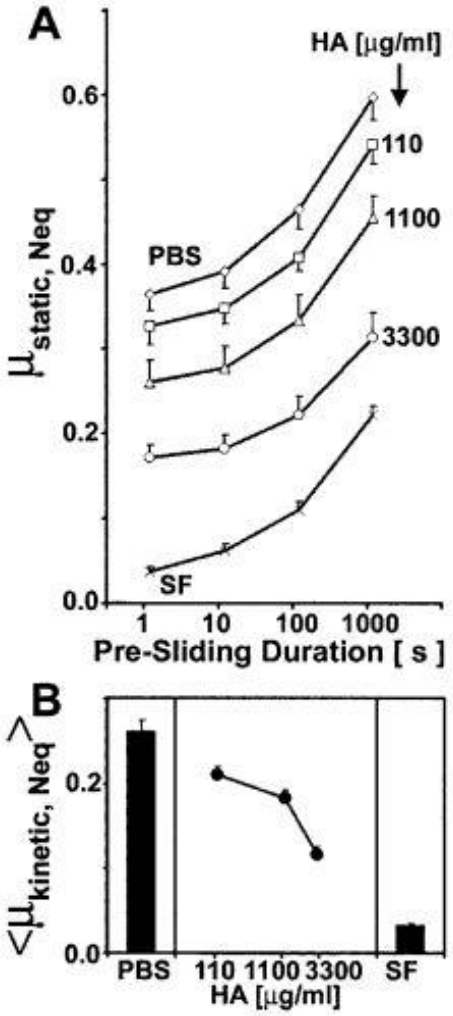

Figure 1-3: Static (**A**) and Kinetic (**B**) coefficient of friction for varying HA concentrations. PBS and SF values are shown for reference[8].

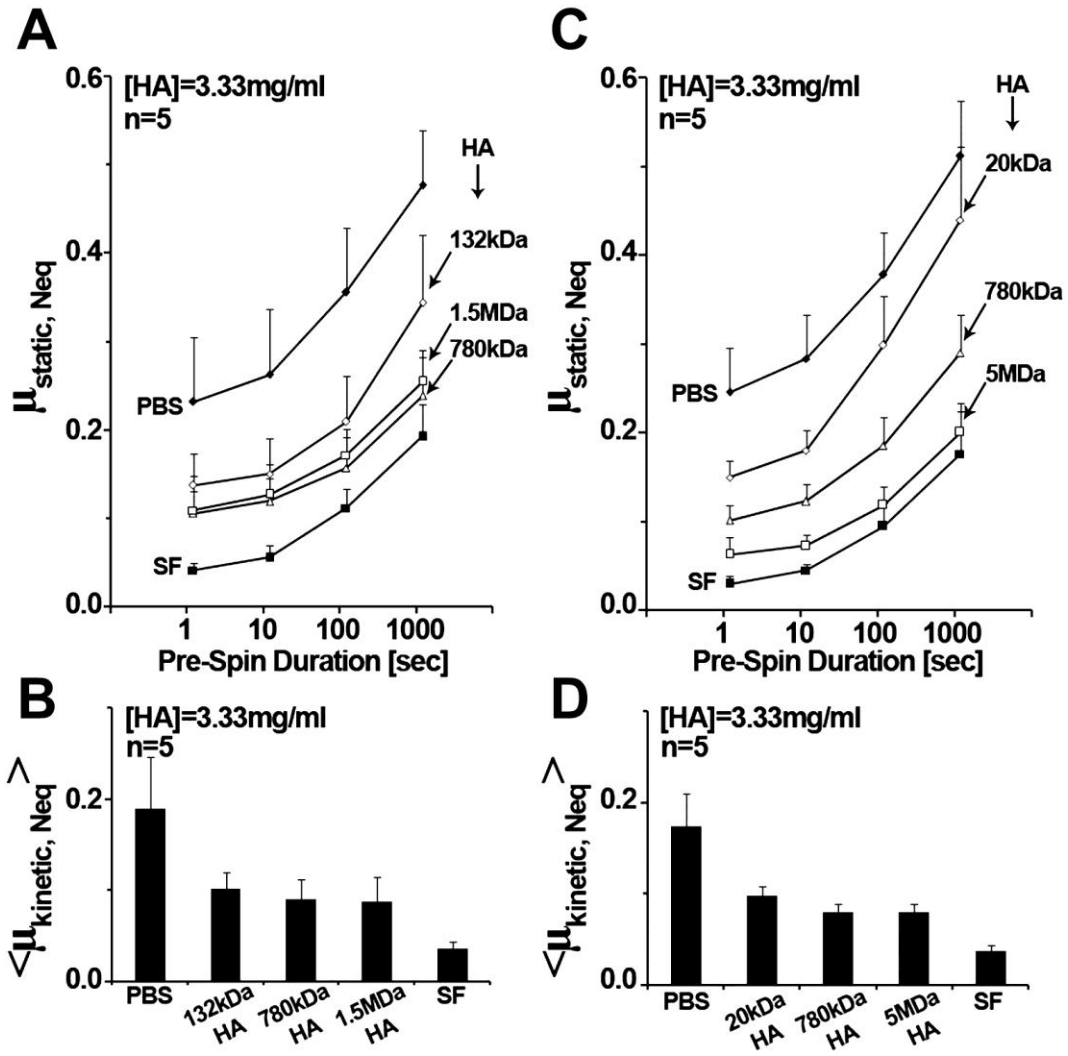

Figure 1-4: Static (**A** and **C**) and Kinetic (**B** and **D**) coefficient of friction for varying HA MW. PBS and SF values are shown for reference[30].

This is important when considering that SF extracted from human OA joints show a lower MW distribution of HA[14]. It has been shown that supplementation with HA injections into the synovium of OA affected joints reduces pain, swelling, and increase mobility for a period of 3-6 months after the injection[31].

1.2.2 PROTEOGLYCAN 4

PRG4 is a proteoglycan present in synovial fluid, and is also known as lubricin, superficial zone protein, and megakaryocyte stimulating factor[32]. It is secreted from chondrocytes within the articulating cartilage as well as synoviocytes within the synovium and synovial membrane [32, 33]. PRG4 is distributed throughout synovial fluid and covers the surface of articulating cartilage[34]. The concentration of PRG4 has been reported at 287 +/- 31.8 µg/ml in healthy human synovial fluid[14]. PRG4 is a mucin-like protein composed of 1404 amino acids giving a total MW of about 150kDa, which increases to approximately 460kDa after post translational addition of O-linked oligosaccharides[35]. Mucins are a family of highly glycosylated proteins which form gels, or mucus, which line epithelial cells in the body[36]. PRG4, while very similar structurally to mucins due to its central mucin like domain with extensive O-linked glycosylations, lacks specific protein sequences at its terminals and the ability to form gels formed by high MW mulitmers. Nevertheless, there is significant overlap between mucin and PRG4 research and findings are often transferable. The geometry of the molecule is a flexible rod 200nm in length and 1-2nm in width[37]. A schematic of PRG4's structure is shown in **Figure 1-5**.

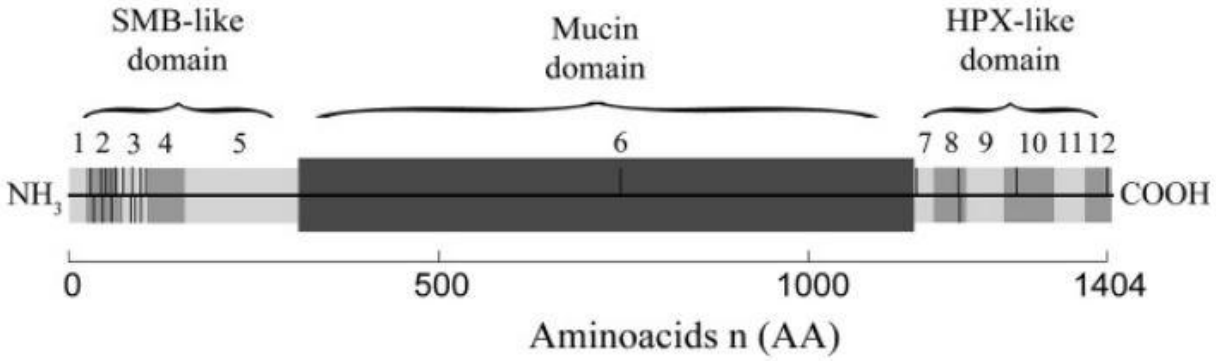

Figure 1-5: A schematic representation of the PRG4 structure. Exons are shown in different shades of gray. Exons 1-5 and 7-12 contain subdomains similar to hemopexin, considered essential binding sites of the molecule[1].

There is a large body of evidence suggesting PRG4 is the dominant macromolecule in boundary lubrication of synovial joints. In a study by Chan, et al. the coefficient of friction of the articular cartilage of both high impact and low impact joints, as measured by atomic force microscopy, was shown to increase significantly after trypsin digestion was used to remove PRG4[28]. It was shown that PRG4 is the most significant macromolecule in comparison to experiments which removed HA or other surface active phospholipids[28]. The results of this study are shown in **Figure 1-6**.

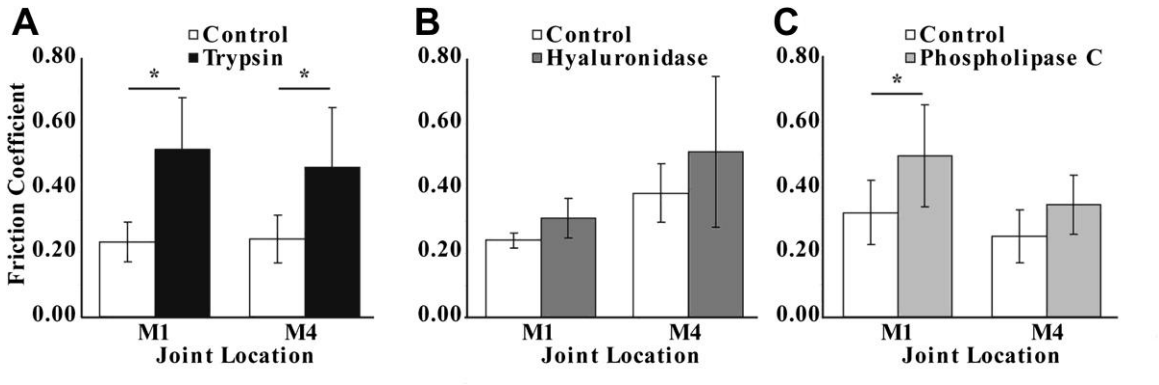

Figure 1-6: Friction coefficients dependence on the removal of PRG4, HA and SALP by trypsin, hyaluronidase and phospholipase C respectively[28].

Experimentation with PRG4 and SF on a cartilage-cartilage interface in a boundary mode of lubrication by Schmidt, et al. showed a significant decrease in the kinetic coefficient of friction from a PBS control[8]. The kinetic coefficient of friction associated with a PRG4 solution of 450µg/ml was reduced to ~0.11 compared to values for PBS (~0.24)[8]. In this study SF generated a mean kinetic coefficient of friction of ~0.025[8]. Results from this study are shown in **Figure 1-7**.

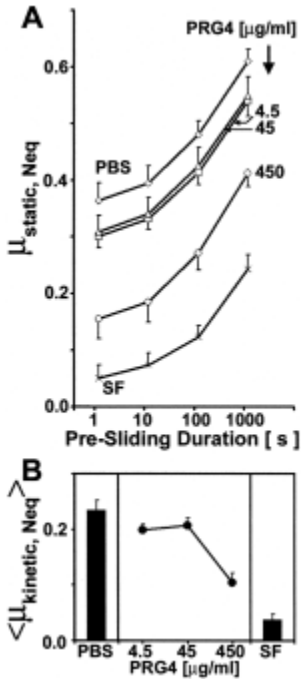

Figure 1-7: Static (**A**) and Kinetic (**B**) coefficient of friction for varying PRG4 concentrations. PBS and SF values are shown for reference[8].

On hydrophobic surfaces like cartilage, PRG4 most likely binds via its hydrophobic N- and C- terminus domains creating an outward loop configuration[38]. It is thought that the outward facing hydrophilic loops from opposing cartilage surfaces repel each other creating the basis for a boundary lubricant. This conformation of adherence to the cartilage is essential. In a study by Zappone, et al. PRG4 is removed from the cartilage surface via proteolytic digestion and lubrication drastically decreased[1]. After digestion the coefficient of friction increased from ~0.6 to ~1.1-1.9[1]. Another study which aimed at elucidating the mechanism of PRG4 boundary lubrication examined the lubrication differences between surface bound PRG4 and soluble PRG4[39]. Results from this study suggest that although both bound and soluble PRG4 increase lubrication in comparison to controls, bound PRG4 was more effective at lubricating the

sample[39]. Further results from this study suggest that using a sample where PRG4 is bound to the articulating cartilage surface and within the solution increases the lubrication even further, providing further evidence that the solution properties of PRG4 can be related to its function as a boundary lubricant[39].

PRG4 can be produced from a variety of methods including: purification of SF (human or animal), culturing of cartilage explants or recombinant methods. The PRG4 used in the Schmidt lab group is produced by harvesting articular cartilage disks from bovine stifle joints (Calgary, AB, Canada) and culturing in the presence of transforming growth factor-β15[5]. The PRG4 is then purified using Diethylaminoethyl (DEAE) anion exchange chromatography and centrifugal filtration[5]. The purity was confirmed using 3–8% Tris-Acetate Sodium Dodecyl Sulfate Polyacrylamide Gel Electrophoresis (SDS-PAGE) followed by protein stain and western blotting using Invitrogen's NuPAGE system (Carlsbad, CA, USA). While this method is practical for lab scale production of PRG4, the product is not human and most likely only 85% purity [40]. More recently, a recombinant human PRG4 (rhPRG4) is being used to produce PRG4 from Chinese hamster ovary cells. This product is genetically human, and manufactured to a much higher purity (~99%) and therefore better represents an eventual end product suitable for human supplementation [40]. rhPRG4 has been shown to contain similar glycosylation patterns as native PRG4, as well as effectively lubricate both articular cartilage and the surface of the eye[40]. The lubrication function of rhPRG4 is in good agreement with lubrication from native PRG4[40].

PRG4 is capable of dimerization via disulfide bonds and is present as a monomer and dimer within SF [41]. Disulphide bonds also contribute to the tertiary structure or folding of the protein, which is essential to the function of the molecule. Reduction and alkylation (R/A) of

PRG4 breaks these disulphide bonds and has been shown to separate multimers into monomers as well as release small fragments from the PRG4 structure (~70kDa) which were most likely attached to the molecule through disulphide bridges. This destruction of the protein structure, especially at the terminal end of the molecule, has been shown to reduce the molecules effectiveness as a boundary lubricant. Previous research has shown that R/A-PRG4 binds less effectively to the PRG4 surface [42, 43].

1.2.3 SYNERGISTIC EFFECTS BETWEEN HA AND PRG4

As discussed before, the role of HA in cartilage boundary lubrication is currently a subject of debate. The implications of a HA+PRG4 complex may help in the understanding of HA's role in boundary lubrication. As early as the 1970's Swann, et al. [44], suggested the low intrinsic viscosity values of HA, which rejects it as a boundary lubricated, could be altered in vivo if the molecule interacts with a protein. In addition to this Jay [45] determines that if HA and PRG4 could bind, PRG4 could help HA bind to the articular surface and aid in the structuring of water around the articular cartilage surface. It is suggested that PRG4 contains a variety of binding domains[34]. The interaction of PRG4 with glycosaminoglycans is possibly mediated through an alleged cationic region located on vitronectin exon 7 [34]. This binding site is also near two hemopexin-like repeats of vitronectin exons 4 and 5 that have the capability to bind to ligands [34]. These and other insights are driving a search for direct evidence of a PRG4+HA interaction.

Although it is assumed that boundary lubrication is the dominant form of lubrication in articular joints under load, a more complex mechanism of lubrication from PRG4 and HA has

been proposed to explain observed phenomena. It has been observed that boundary friction decreases with increasing mucin concentration, due to an increase in thickness of the mucin layer which covers the articular cartilage surface creating a viscous boundary lubricant layer[5]. The resulting increase in lubrication is suspected to be a result of the local viscosity of this viscous boundary lubricant layer and not the overall bulk viscosity of solution[5]. This phenomenon relates boundary lubrication to the hydrodynamic properties of this micro layer of mucins, such as PRG4, which infers that the properties of PRG4, and possibly HA, in solution can be directly related to their function as a boundary lubricant.

Proof of an interaction in solution or at the cartilage surface has been elusive. In a study by Schmidt, et al. the combination of HA and PRG4 was shown to reduce the coefficient of friction between two cartilage surfaces more than either molecule individually[8]. The observed coefficient of friction from a HA and PRG4 medium approached the coefficient of friction generated from SF[8]. This effect is shown in **Figure 1-8**. Another study demonstrated that supplementing 3mg/ml solutions of HA of varying MW with PRG4 increased the lubricity of the sample[30]. In this experiment, the synergistic effect was not a function of the HA MW[30].

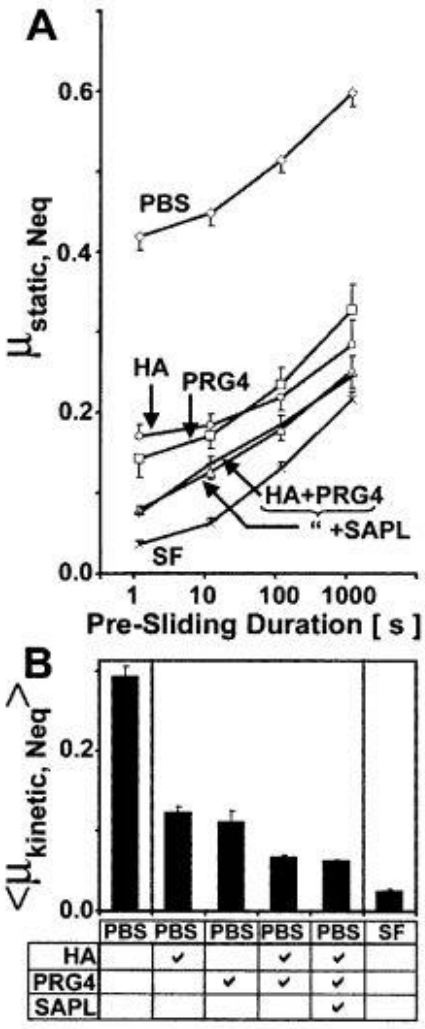

Figure 1-8: Static (**A**) and Kinetic (**B**) coefficient of friction for PRG4, HA and HA+PRG4. PBS and SF values are shown for reference [8].

It is evident that there is a functional interaction between HA and PRG4, but little is known about the mechanistic nature of this interaction. A number of studies have been attempted to find direct evidence of an interaction in varying ways, most of them focusing on elucidating the interaction within solution. A technique used to find direct evidence of a PRG4 and HA interaction is the use of electrophoretic mobility shift assay (EMSA) [30]. This technique

operates under the assumption that a complex is larger and therefore less mobile than two separate components[30]. Using EMSA it was determined that the motion of 150kDa and 1000kDa HA through an agarose gel was retarded by PRG4, suggesting a weak interaction between HA and PRG4 in solution[30].

A multiple-particle-tracking micro-rheology (MPTM) technique was used to determine an interaction between HA and PRG4[2]. The technique tracks the diffusion of fluorescently labeled tracers within normal and PRG4 deficient SF using a fluorescence microscope[2].The diffusive behavior of the tracer was characterized by measuring the ensemble-averaged mean-squared displacement which is related to the diffusion coefficient[2]. By analyzing the motion of these tracers, it was suggested that PRG4 deficient SF lacks the sub diffusive and elastic properties associated with normal SF[2]. It is implied that without PRG4, the HA in SF adopts a more rigid conformation which is unable to layer and demonstrate shear thinning[2]. Results from the experiment suggests that PRG4 creates entanglements within the HA matrix[2]. While this experiment reveals valuable information about the nature of PRG4 in HA containing SF, it looks specifically at the nature of PRG4 within SF. This top down approach gives little information into the concentration dependence of the HA-PRG4 interaction, as well as the importance of HA MW.

A third method that has been applied to observing an interaction between HA and PRG4 is single molecule microscopy. Single molecule microscopy is a highly sensitive technique which allows for the tracking of individual fluorescent molecules in a resolution within milliseconds[46]. Single molecule microscopy was used to observe the motion of HA in human SF, and found evidence of interaction between HA and the SF matrix[46]. This was performed by analyzing the motion of HA in comparison to a dextran tracer control molecule[46].

1.3 CONFOCAL FRAP

1.3.1 CONFOCAL FRAP OVERVIEW

Confocal fluorescence recovery after photobleaching (FRAP) is a technique used to study two-dimensional lateral diffusion of fluorescent particles. The technique allows for study of a solution's macroscopic diffusive properties instead of the more local and microscopic properties observed with MPTM or single molecule microscopy. FRAP also allows for the analysis of any fluorescently labeled molecule and not just tracers, which is the case for MPTM.

The method is performed by exposing a small region of fluorescently labeled molecules to a brief intense pulse of light causing irreversible photobleaching within the region (loss of fluorescence). Transport coefficients can then be determined by observing the recovery of fluorescence into the photobleached region, as measured by a confocal microscope. Confocal FRAP allows for: determination of diffusion rates and coefficients, detection of a diffusive or systematic transport, and as a way to determine the amount of immobile fluorophores.

1.3.2 CONFOCAL FRAP ANALYSIS METHODS

There are a variety of methods of analysis for FRAP experiments, mostly depending on the computing power available at the time of development. Early FRAP experiments tracked the fluorescent intensity of the central bleached area over time. This analysis is idealized in **Figure 1-9**, and a time series of images from a performed experiment is shown in **Appendix B**.

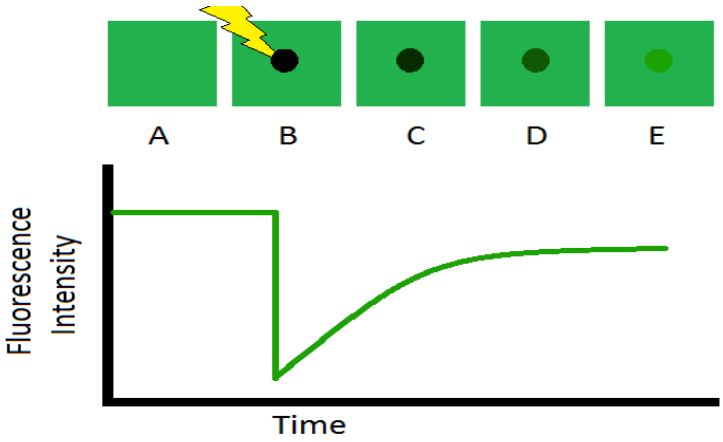

Figure 1-9: A graphical and pictorial representation of a FRAP experiment.

In the analysis displayed in Figure 9, the first component of the graph (section A) represents a period of pre-bleach monitoring. This pre bleach monitoring is used to normalize the graph to small amounts of photo bleaching which occurs during monitoring. In Figure 9, the graph has already been normalized, and therefore the initial section has a slope of 0. After the pre-bleach monitoring the photo bleaching by the high intensity laser (section B) causes the intensity of fluorescence to rapidly decrease. The curve shown in sections C-E then shows the recovery of fluorescence to a final resting state. For the simplest analysis, the curve generated during the recovery can be fit to an exponential model (Equation 1) through a least squares fitting method.

$I = IE - I_1 \cdot \exp\left(-\frac{t}{T_1}\right)$ **(1)**Where I is the intensity of the fluorophores, T_1 is the characteristic time of recovery and I_1 is a constant. For a circular, Gaussian bleaching profile in the absence of flow, $T=\omega^2/4D_t$, where ω is the half width of the e^{-2} value of the Gaussian and D_t is the diffusion coefficient.[47].

The previous discussed method, while valid, is a very simplistic approach which can often miss fast recovery times, for example on the order of 10^{-8} cm^2 s^{-1}. A more complex method was developed by Kubitscheck et al. 1994 [48], and used by Gribbon et al. 1999 [48, 49], to analyze FRAP experiments looking at HA solutions. Using this method data collected from the frap experiment are obtained as a series of images representing the FRAP experiment. To summarize the method, the image time series are processed with a 3x3 Gaussian filter to remove high frequency noise and correct for saturated pixels. The images are then scaled to the average pre-bleach intensity and normalized to small amount of photobleaching which occurs during monitoring of the recovery. The radial average of intensity for each image is then computed to generate Gaussian plots for every time point representing the distribution of intensity from the center of the image (**Figure 1-10**).

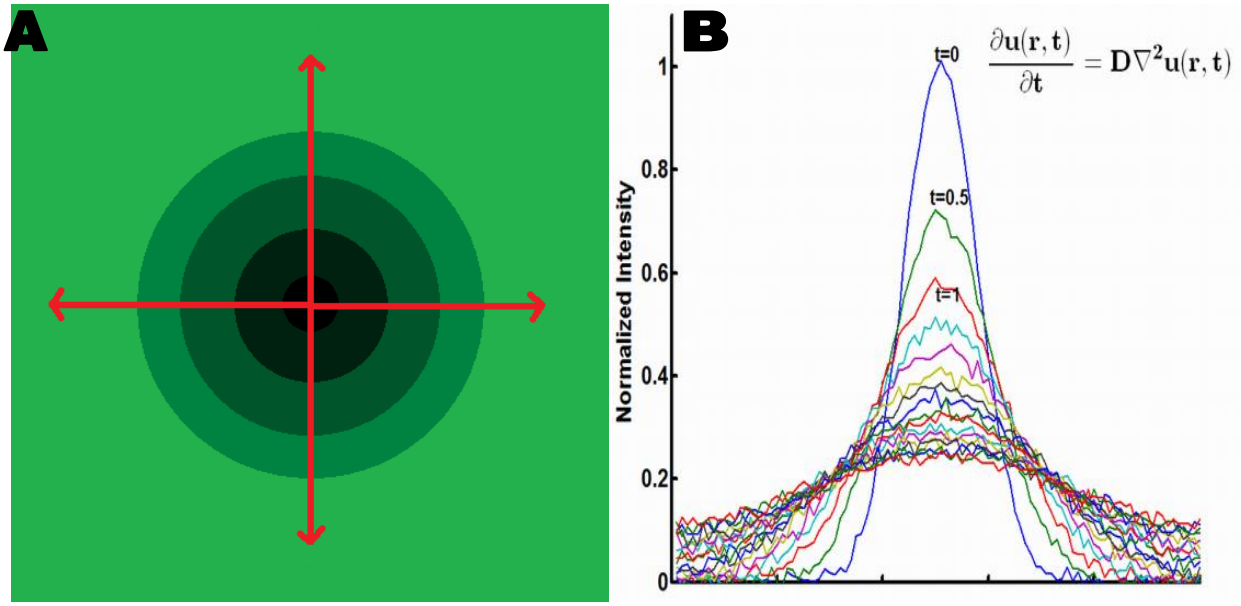

Figure 1-10: The radial average of the fluorescent intensity from the center of the FRAP image (**A**) is computed for every time point to generate a time series of Gaussians (**B**)

From the radial distribution function the sum of the two second central moments, $\mu_{(2,i)}$, is determined. As shown in the by Kubitscheck et al. 1994 paper [48], it has been shown that the sum of the two second central moments is linearly related to the lateral diffusion coefficient D and the mobile fraction k. The mobile fraction is simply calculated according to the equation k=(F(∞)-F(0))/(F_0-F(0)), where F(∞) represents the final equilibrium fluorescent intensity after bleaching, F(0) represents the fluorescent intensity at immediately after bleaching and F_0 represents the initial pre-bleach fluorescent intensity. D_t will therefore be calculated by fitting a line to the initial linear portion of $\mu_{(2,i)}$ and dividing the slope by k.[48].

The Kubitschek et al. method [48] relies on the linear relationship of $\mu_{(2,i)}$ of the Gaussian series to D_t. This method simplifies and lowers the computing power necessary for data analysis, but relies on determining the linear portion of the second central moment with respect to time, which can vary with experimental data. With modern computing power, an analysis program can be written which directly fits the time development of the Gaussians to the Bessel expansion solution of the cylindrical diffusion equation (Equation 2)[50].

$$u(r,t) = \sum_{1=n}^{\infty} C_n e^{\frac{\lambda_n{}^2 D_t t}{R^2}} J\left(\frac{\lambda_n r}{R}\right) \quad \textbf{(2)}$$

Where u is the scaled intensity of the fluorescence, r is the radius, t is time, C_n is defined in Equation 3, J_n is the n order Bessel function, D_t is the lateral diffusion coefficient R is the total radius of the photo bleached area, and λ_n is the n^{th} root of J_0.

$$C_n = \sum_{1=n}^{\infty} \frac{\int_0^R r J_0\left(\frac{\lambda_n r}{R}\right) f(r) dr}{\frac{R^2}{2}[J_0(\lambda_n)]^2} \quad \textbf{(3)}$$

Where f(r) is the initial condition. This method relies on an iterative fitting method which approximates the series of Gaussian profiles as a Bessel function to determine the fitted value for D_t, the lateral diffusion coefficient. This analysis method, and subsequent Matlab program, was developed by Michael Samsom (PhD student in the Schmidt Lab) specifically for this project. The method is based on the Kubitschek method and cylindrical diffusion analysis from Carslaw et al.[48, 50].

1.3.3 PREVIOUS CONFOCAL FRAP EXPERIMENTS ON HYALURONAN

In a classic study by Gribbon, et al. confocal FRAP was used to determine the intermolecular hydrogen bonding, electrostatic interactions and matrix fluidity of HA solutions[49]. The experiment involves characterizing the diffusion of HA, as well as a FITC-labeled tracer, through solutions of HA under a variety of conditions. The diffusion of 500kDA HA and 839kDa HA was determined to have a free diffusion coefficient of $7.9 \times 10^{-8}\ cm^2\ s^{-1}$ and $5.6 \times 10^{-8}\ cm^2 s^{-1}$ respectively[49]. When electrolytes were added to induce coil contraction within HA and de-stiffen the matrix, the resulting self-diffusion was increased 2.8-fold[49]. Alkaline conditions, which disrupt hydrogen bonds, resulted in further increase of self-diffusion[49]. From these results it can be inferred that stiffening of molecules and removing hydrogen bonds makes the HA matrix more fluid and dynamic allowing for increased self-diffusion[49]. Diffusion of a 2000kDa FITC-dextran tracer was determined to be

higher for lower MW HA at low HA concentrations, but independent of HA MW at high concentrations of HA (~6mg/ml)[49]. The tracer in PBS at the zero concentration HA was 13.1±0.5 x 10^{-8} cm^2s^{-1} to approximately 6 x 10^{-8} cm^2s^{-1} at 4mg/ml HA. The results for tracer diffusion at the different HA concentrations can be fit to the universal scaling equation for tracers (Equation 4).

$$D_t = {D_t}^0 \exp(-\beta c^\gamma) \quad \textbf{(4)}$$

Where ${D_t}^0$ is the zero concentration HA diffusion value, c is the HA concentration, and β and γ are empirical constants[51]. Further, the empirical constants can be used, with the hydrodynamic diameter of the tracer d, to determine the apparent mesh size of the HA matrix. This is calculated in Equation 5[52].

$$\xi = \left(\frac{d}{\beta}\right) c^{-\gamma} \quad \textbf{(5)}$$

Using a tracer within HA solutions allows for insight into the diffusivity and structure of the HA polymer matrix. Additionally, FRAP's ability to study the diffusion of any fluorescently labeled molecule allows for the eventual study of HA diffusion properties and not just the behaviour of a tracer. Using a dextran tracer Gribbon et al. was able to determine the permeability of HA solutions and calculate the apparent mesh sizes of the generated networks. If PRG4 creates an entanglement between HA polymers, as suggested in the research of Jay et al. [2], the resulting decrease in permeability should be measurable using confocal FRAP. It is therefore evident that

confocal FRAP is an ideal method to study PRG4 and HA interactions which remain poorly understood.

1.4 THESIS OBJECTIVES

The objective of this thesis was to determine whether PRG4 will affect the permeability of simple HA solutions due to specific interactions between PRG4 and HA polymers in solution. It is hypothesized that the specific PRG4-HA interactions will reduce the mesh size of the HA network, significantly decreasing the permeability of the solutions. Additionally, the results from analyzing simple HA solutions will be compared to the more complex SF to demonstrate a physiological change from altered SF composition. This hypothesis will be tested by the following aims:

Aim 1: Determine whether PRG4 (at physiological and pathophysiological concentrations) affects the permeability of HA solutions of different concentrations and MW. (Chapter 2)

Aim 2i: Determine whether the effect of PRG4 is specific by ascertaining if BSA (at physiological and pathophysiological concentrations) also affects the permeability of HA solutions of different concentrations and MW. (Chapter 2)

Aim 2ii: Investigate whether the effect of PRG4 is specific to PRG4`s tertiary/quaternary protein structure by comparing the effect of native PRG4 reduced and alkylated PRG4 to reveal the importance of PRG4's tertiary and quaternary protein structure. (Chapter 2)

Aim 3i: Determine whether rhPRG4 replicates the permeability effects of bovine PRG4 (at physiological and pathophysiological concentrations) on HA solutions of different concentrations and MW. (Chapter 3)

Aim 3ii: Measure the permeability of normal and pathological SF samples and determine the effect of supplementation of rhPRG4 on the SF samples permeability (Chapter 4)

CHAPTER 2: INVESTIGATING THE EFFECT OF PROTEOGLYCAN 4 ON HYALURONAN SOLUTION PROPERTIES USING CONFOCAL FLUORESCENCE RECOVERY AFTER PHOTOBLEACHING

2.1 ABSTRACT

Objectives: (1) use confocal fluorescence recovery after photobleaching (FRAP) to examine the specific and dose-dependent effect of proteoglycan 4 (PRG4) on hyaluronan (HA) solution networks by analyzing the diffusion of a FITC-dextran tracer through HA solutions of different molecular weight; (2) assess the effect of reduction and alkylation (R/A) of PRG4 on its observed effects on HA solutions at different concentrations.

Methods: Confocal FRAP was used to determine the diffusion coefficient of FITC-dextran tracers (D_t) through 1500kDa and 500kDa HA solutions (0 to 3.3mg/ml) ±PRG4 or a control protein, Bovine Serum Albumin (BSA), at physiological (450μg/ml) or pathophysiological (45μg/ml) concentrations. The effect of either PRG4 or R/A PRG4 at physiological or pathophysiological solutions on 1500kDa HA solutions (0 to 3.3mg/ml) was also investigated. Empirical constants from fitting data to the universal scaling equation was used to calculate the average distribution of apparent mesh sizes.

Results: PRG4 at both 45 and 450μg/ml slowed the diffusion of the FITC-dextran tracer for all concentrations of HA and caused a decrease in the calculated apparent mesh size, or average pore size, within the HA solution network. This effect was specific to PRG4, not observed with the control protein BSA, but not dependent on its tertiary/quaternary structure as the effect remained after R/A of PRG4. In all experiments, tracer diffusion reduced with increasing HA concentrations according to a stretched exponential model.

Conclusions: These results indicate that PRG4, at both physiological and pathological concentrations, can significantly alter the solution properties of HA; PRG4 essentially reduced the permeability of the HA network. This effect may be due to PRG4 entangling HA molecules through binding and/or HA crowding PRG4 molecules into a self-assembled network impeding the diffusion of the FITC-dextran tracers. The mechanism of this PRG4 + HA interaction in solution remains to be completely elucidated.

2.2 INTRODUCTION

Hyaluronan (HA) is a vital macromolecular component of synovial fluid (SF) with a variety of important functions. HA is a negatively charged biopolymer composed of alternating D-glucuronic acid and N-acetylglucosamine that forms dynamic networks in solution[22]. The molecule exists in SF at molecular weights (MW) between 0.2 to 6 MDa, and concentrations of 1-4 mg/ml[2, 53]. A major role of HA in SF is to impart fluid viscosity and elasticity to help transfer loads across the cartilage within the articulating joint[20]. HA has also been shown to effectively reduce friction in dose dependant manner at a cartilage-cartilage biointerface under boundary mode lubrication[8, 30, 34].

Proteoglycan 4 (PRG4) is a mucin like glycoprotein also present in SF and covering the surface of articulating cartilage[34]. PRG4 is considered a mucin like protein due to the post translational addition of O-linked oligosaccharides and has an apparent molecular weight (MW) of approximately 460kDa[54]. The geometry of the molecule is a flexible rod 200nm in length and 1-2nm in width[37]. PRG4 has been reported at an average concentration of 287 +/- 31.8µg/ml in healthy human SF, though it can vary substantially from 129 to 450µg/ml[14]. PRG4 has been shown to effectively reduce friction in a dose dependent manner at a cartilage-cartilage biointerface under boundary lubrication[8], as well as at cartilage-glass and latex-glass surfaces [34, 55]. PRG4 is capable of dimerization via intramolecular disulfide bonds and exists in SF in both monomeric and dimeric forms[41]. Reduction and alkylation (R/A) of PRG4, and disruption of both intra and inter molecular disulfide bonds, has been shown to reduce multimers into monomers and release small fragments from the PRG4 structure (~70kDa)[41, 56]. This

results in a significant reduction in binding of PRG4 to the surface of articular cartilage and an associated reduction in its cartilage boundary lubricating ability[42, 43, 45].

In addition to functioning as lubricants individually, PRG4 and HA also function together synergistically at the cartilage surface and possibly in solution within SF. When combined in solution at physiological concentrations PRG4 and HA reduce friction at a cartilage-cartilage biointerface under boundary lubrication to lower levels than either macromolecule independently, approaching the lubrication of healthy SF[8, 30]. This functional synergism has been demonstrated at physiological concentrations with various MW HA without any significant variation in lubricating ability[30]. This synergism suggests at least a functional interaction between HA and PRG4 at the cartilage surface, and possibly in solution as well; though interactions of macromolecules need not be the same at a surface and in solution.

Multiple studies have attempted to elucidate the mode of interaction of PRG4 and HA in solution, and thus potentially contribute to the understanding of their SF like synergistic cartilage boundary lubricating ability[2, 30, 46]. An electrophoretic mobility shift assay demonstrated evidence of a weak interaction when the motion of PRG4 and HA was retarded through an agarose gel in comparison to the individual components[30]. Additionally, evidence for an interaction in solution has been reported using a multiple-particle-tracking microrheology (MPTM) technique to study the effect PRG4 has on the biophysical properties of SF (a semi dilute HA solution)[2]. Experimentation performed on healthy as well as PRG4-deficient SF suggested that PRG4 creates a network of "entanglements" within HA-containing SF, which results in an increased relaxation time for SF[2]. Despite these results, the specific mechanism and concentration dependence of this interaction has yet to be determined. A more detailed understanding of HA and PRG4 interaction in solution could help explain the molecular basis of

the biophysical properties of normal and pathological SF. Accordingly, an experimental technique which allows us to probe the biophysical properties of complex HA and PRG4 solutions would be valuable.

Confocal fluorescence recovery after photobleaching (FRAP) is a microscopic technique that has been used to investigate solution properties and molecular networks of HA[48]. Confocal FRAP provides a powerful tool for studying concentrated and complex polymer solutions in the absence of shear stress[57]. The technique requires only a small volume of a sample (35µl), and can be used to determine solutions properties under varying environmental factors. Gribbon et al.[49] used FRAP to determine how electrolyte concentration and pH affect the hydrogen and electrostatic intramolecular bonds within the repeat sugar subunits of HA. The resulting change in intramolecular bonding was shown to change the stiffness, and contraction of the HA molecules, and thus network formation. Due to confocal FRAP's ability to reveal details about the structure of HA as well as the HA network as a whole, it is an ideal method to evaluate the specific and dose-dependent affect PRG4 has on HA solution properties.

Therefore, the objectives of this study were to 1) use confocal FRAP to examine the specific and dose-dependent effect of PRG4 on HA solution networks by analyzing the diffusion of a FITC-dextran tracer through HA solutions of different MW, and 2) assess the effect of R/A on PRG4, and hence altered tertiary/quaternary structure, on its observed effects on HA solutions at different concentrations.

2.3 MATERIALS AND METHODS

2.3.1 MATERIALS

HA, 1500kDa and 500kDa, was obtained from LifeCore Biomedical (Chaska, MN, USA), and the MW was qualitatively confirmed (**Figure 2-1**) by 1% agarose gel electrophoresis (AGE)[30]. FITC-dextran (MW= 2000 kDa) and bovine serum albumin (BSA) were obtained from Sigma-Aldrich (St. Louis, MO, USA). The hydrodynamic radius of the FITC-dextran tracer was determined using dynamic light scattering to be 19.50± 1.29nm (mean ± SEM, n=3), which is in good accordance with reported values[49]. All samples were prepared in PBS.

PRG4 was prepared using previously described methods[8]. Briefly, articular cartilage disks were harvested from bovine stifle joints obtained from a local abattoir (Calgary, AB, Canada) and cultured for 28 days, with media changes every 3 days, in the presence of transforming growth factor-β1[8]. The PRG4 was than purified from PRG4 rich media using Diethylaminoethyl anion exchange chromatography and centrifugal filtration[8]. The purity was confirmed using 3–8% Tris-Acetate Sodium Dodecyl Sulfate Polyacrylamide Gel Electrophoresis (SDS-PAGE) followed by protein stain and western blotting using Invitrogen's NuPAGE system (Carlsbad, CA, USA). The concentration was then determined by bicinchoninic acid assay (BCA) (Thermo Fisher Scientific; Rockford, IL, USA). R/A PRG4 was prepared by incubating in PBS with 10mM dithiothreitol for 2h at 60C and 8.5pH and then 40mM iodoacetate for 2h at room temperature[41]. The R/APRG4 was recovered by dialyzing against PBS for 12h at 37C with the PBS being changed for a fresh solution after 6 hours. R/A of PRG4 was confirmed through SDS-PAGE followed by protein staining.

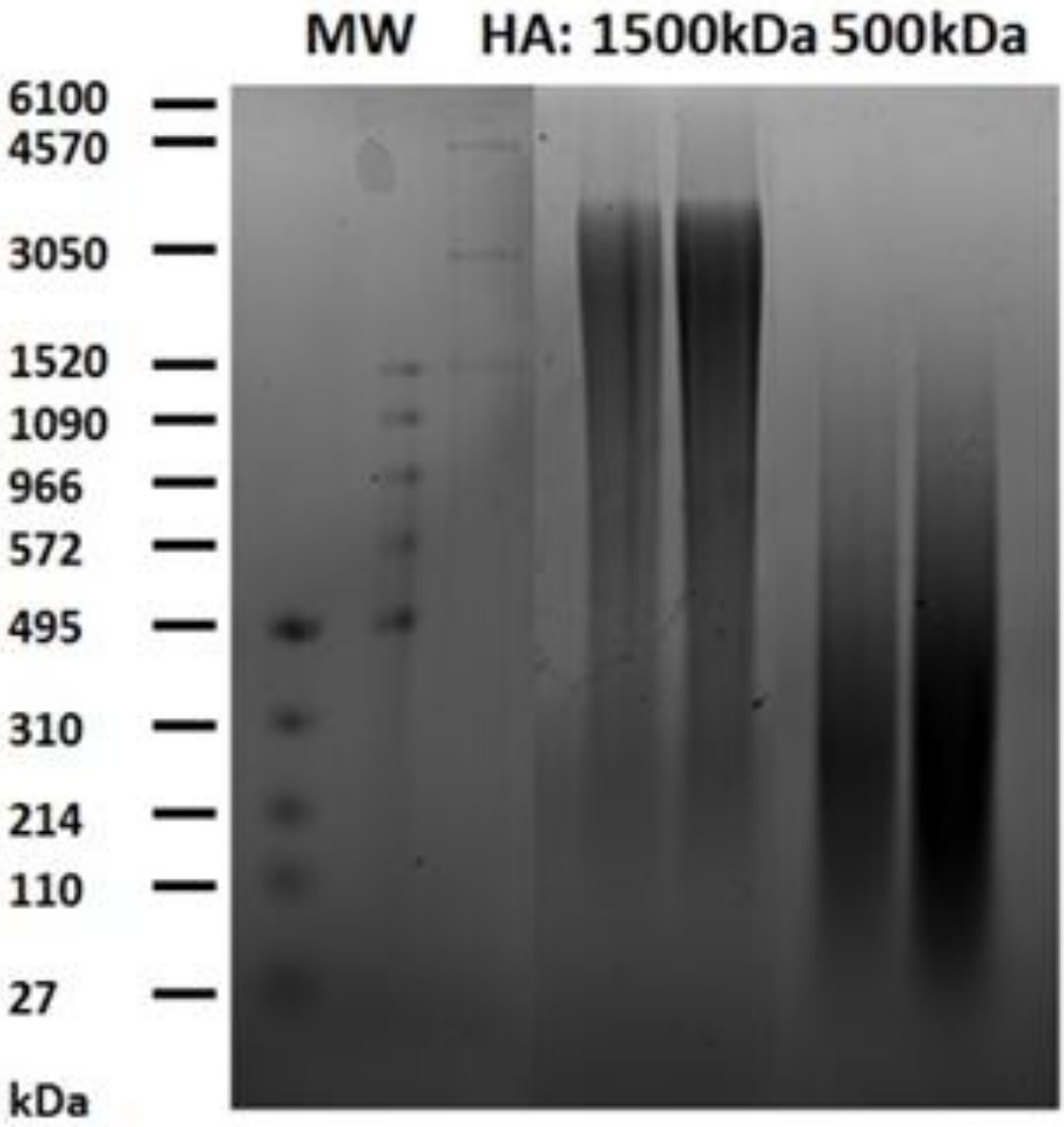

Figure 2-1: MW characterization of HA used in confocal-FRAP studies via agarose gel electrophoresis.

2.3.2 SAMPLE PREPARATION

HA Concentration Series: 1500kDa and 500kDa HA solutions were prepared in experimental sets of concentrations 0, 0.1, 0.3, 1 and 3.3mg/ml. FITC-dextran was added into every HA solution to a final concentration of 0.1mg/ml.

HA±PRG4: After preparation of a 1500 and 500kDa HA concentration series (0, 0.1, 0.3, 1 and 3.3mg/ml solutions), each HA solution was divided into two samples. One half of the HA samples was added to a dried mass of PRG4 to a final concentration of either 450µg/ml or 45µg/ml to make the HA+PRG4 solution series, while the other half of the HA solutions remained unaltered as the HA-PRG4 solution series

HA±BSA: HA±BSA solutions were made in the exact same way as HA±PRG4 solutions except powdered BSA was added in the place of PRG4.

HA+ PRG4 vs. HA+ R/A PRG4: After preparation of a 1500 and 500kDa HA concentration series (0, 0.1, 0.3, 1 and 3.3mg/ml solutions), each HA solution was divided into two samples. One half of the HA samples was added to a dried mass of PRG4 to a final concentration of either 450µg/ml or 45µg/ml to make the HA+PRG4 solution series, while the other half of the HA solutions was added to a dried mass of R/A PRG4 to a final concentration of either 450µg/ml or 45µg/ml to make the HA+R/A PRG4 solution series.

2.3.3 CONFOCAL FRAP PROTOCOL

Samples were mounted and sealed onto concave depression slides (Pearl, China). The prepared samples were subjected to confocal FRAP experiments performed on a Ziess LSM 780 scanning confocal microscope essentially as described in previous studies[49]. The microscope was set to a pixel size of 0.19µm and a pixel dwell time of 0.79µsec. The pinhole was set to the maximum value to observe an optical section of 33 µm. A 40x objective lens (NA=1.1) was used. A 96.5x96.5µm area was monitored by a 489nm 100mW diode laser at 0.2% maximum power for 20 scan cycles. The 489nm 100mW diode laser was then used in tandem with a 405nm 100mW diode laser, both at 100% maximum power, to bleach a central circle with a diameter of 19µm for 20 scan cycle iterations. The post bleach sample was then monitored by the 489nm 100mW diode at 0.2% maximum power for a total of 600 cycles.

2.3.4 DATA ANALYSIS

The obtained images were analyzed by directly fitting the time dependent bleaching intensity profiles to the Bessel expansion solution of the cylindrical diffusion equation (**Equation 2**)[50].

$$u(r,t) = \sum_{1=n}^{\infty} C_n e^{\frac{{\lambda_n}^2 Dt}{R^2}} J_1\left(\frac{\lambda_n r}{R}\right) \quad \textbf{(2)}$$

Where u is the scaled intensity of the fluorescence, r is the radius, t is time, C_n is defined in **Equation 3**, J_n is the n order Bessel function, D is the lateral diffusion coefficient, R is the total radius of the photo bleached area, and λ_n is the n^{th} root of J_0.

$$C_n = \sum_{1=n}^{\infty} \frac{\int_0^R r J_0\left(\frac{\lambda_n r}{R}\right) f(r) dr}{\frac{R^2}{2}[J_0(\lambda_n)]^2} \quad \textbf{(3)}$$

Where f(r) is the initial condition.

In summary, the image time series were processed with a 3x3 Gaussian filter to remove high frequency noise. The fluorescent intensity at the corners of the images were used to scale the images to ambient photobleaching, which occurs during monitoring of the images. The radial average of intensity for each image was determined to generate one dimensional radial intensity vectors for every time point which represented the distribution of fluorescent intensity from the center of the image. D was than determined using the Bessel expansion solution of the cylindrical diffusion equation (Equation 1) to directly fit the time development of the experimental data using a Levenberg–Marquardt algorithm, with the initial condition set to the initial bleaching profile at t=0. The R^2 value for fitting the Bessel Expansion solution to the time development of the Gaussians was greater than 0.99 for all measured image time series.

For all experimental sets (0.1 to 0.3 mg/ml HA) the calculated diffusion coefficients were fit to the tracer diffusion scaling equation (**Equation 4**) using a least squares optimization[51].

$$D_t = {D_t}^0 \exp(-\beta c^{\gamma}) \quad \textbf{(4)}$$

Where D_t is the lateral diffusion coefficient of the tracer, D_t^0 lateral diffusion coefficient of the tracer in PBS (free diffusion coefficient of the tracer), c is the concentration of the polymer, and β and ν are empirical constants [51]. β typically relates to the inter polymer hydrodynamic interaction between the tracer and the polymer matrix, while deviations of ν from 1 relate to contraction of the polymer at high concentrations [49]. When fitting the data sets to the universal scaling equation the D_t^0 was set as a free parameter. The empirical constants from the scaling equations were used to calculate the average distribution of apparent mesh sizes, ξ, using the correlation length relation (**Equation 5**) [52].

$$\xi = (\frac{d}{\beta})c^{-\nu} \quad (5)$$

Where d is the hydrodynamic diameter of the tracer. All calculations and image processing was performed with Matlab® (MathWorks, USA).

2.3.5 STATISTICAL METHODS

A total of 4 independent samples were measured for every data point (N=4), with the exception of the HA + PRG4 vs. HA + R/A PRG4 (450μg/ml) where a total of 5 independent samples were measured (N=5). The diffusion coefficient calculated for each independent sample was the result of 6 averaged experiments at various points on the concave microscope slide (n=6). All confocal FRAP measurements for an experimental set (i.e. 0 to 3.3mg/ml ±PRG4) were performed on the same day to reduce extraneous variables. Thus an HA concentration

series was compared to an identical HA series, at the same time of day, with the exception of the additive added to the respective HA concentration set (PRG4, BSA or R/A PRG4). Experiments determining D_t^0 for 2000kDa FITC-dextran were also performed individually and specifically for each experimental set. The effect of HA concentration and added protein (PRG4 or BSA) on the diffusion coefficients was assessed using a two factor ANOVA with α set to 0.05.

2.4 RESULTS

2.4.1 HA±PRG4

PRG4 at 450μg/ml slowed the diffusion of the FITC-dextran tracer for all concentrations of HA and therefore had an effect on the HA solution network. For 1500kDa HA ± 450μg/ml PRG4, the diffusion of the tracer was significantly affected by HA concentration ($p<0.01$) and the presence of PRG4 ($p<0.05$), with no interaction effect ($p=0.779$) (**Figure 2-2A**). Similarly for 500kDa HA ± 450μg/ml PRG4, the diffusion of the tracer was significantly affected by HA concentration ($p<0.01$) and the presence of PRG4 ($p<0.05$), with no interaction effect ($p=0.854$) (**Figure 2-2B**). For all experimental sets there is a clear negative exponential decrease in diffusivity for the tracer as HA concentration increases. The negative exponential trend observed for each increasing HA concentration series (±PRG4) was modeled using the universal scaling equation (**Equation 4**), with a R^2 value of greater than 0.95. The addition of PRG4 at 450μg/ml caused an average decrease in D_t of $1.592 \times 10^{-8}\, cm^2\, s^{-1}$, in 1500kDa HA, and $1.068 \times 10^{-8}\, cm^2\, s^{-1}$, in 500kDa HA, both of which were significant ($p < 0.05$ for both). The measured D_t^0 for the FITC-dextran tracer was $21.04 \pm 0.99 \times 10^{-8}\, cm^2\, s^{-1}$, and $21.64 \pm 1.09 \times 10^{-8}\, cm^2\, s^{-1}$, for 1500kDa and 500kDa respectively.

A significant effect of PRG4 at 45μg/ml on the HA solution network was also observed. For 1500kDa HA ± 45μg/ml PRG4, the diffusion of the tracer through 1500kDa HA was significantly affected by HA concentration ($p<0.01$) and the presence of PRG4 ($p<0.01$), with no interaction effect detected ($p=0.177$) (**Figure 2-2C**). Similarly for 500kDa HA ± 45μg/ml PRG4, the diffusion of the tracer was significantly affected by HA concentration ($p<0.01$) and the presence of PRG4 ($p<0.05$), with no interaction effect detected ($p=0.646$) (**Figure 2-2D**). Also similar to the experimental sets ± 450μg/ml PRG4, for all experimental sets there is a clear negative exponential decrease in diffusivity for the tracer as HA concentration increases, and the negative exponential trend observed for each increasing HA concentration series (±PRG4) was modeled using the universal scaling equation (**Equation 4**), with a R^2 value of greater than 0.95. There does not appear to be a change in tracer diffusivity between the 1500kDa and 500kDa HA The addition of PRG4 at 45μg/ml in 1500kDa HA caused an average decrease in D_t of $1.011 \times 10^{-8}\, cm^2\, s^{-1}$, in 1500kDa HA, and $1.263 \times 10^{-8}\, cm^2\, s^{-1}$, in 500kDa HA, both of which were significant ($p < 0.01, 0.05$ respectively). The measured D_t^0 for the FITC-dextran tracer was $20.04 \pm 0.40 \times 10^{-8}\, cm^2\, s^{-1}$, and $20.18 \pm 0.44 \times 10^{-8}\, cm^2\, s^{-1}$, for 1500kDa and 500kDa respectively.

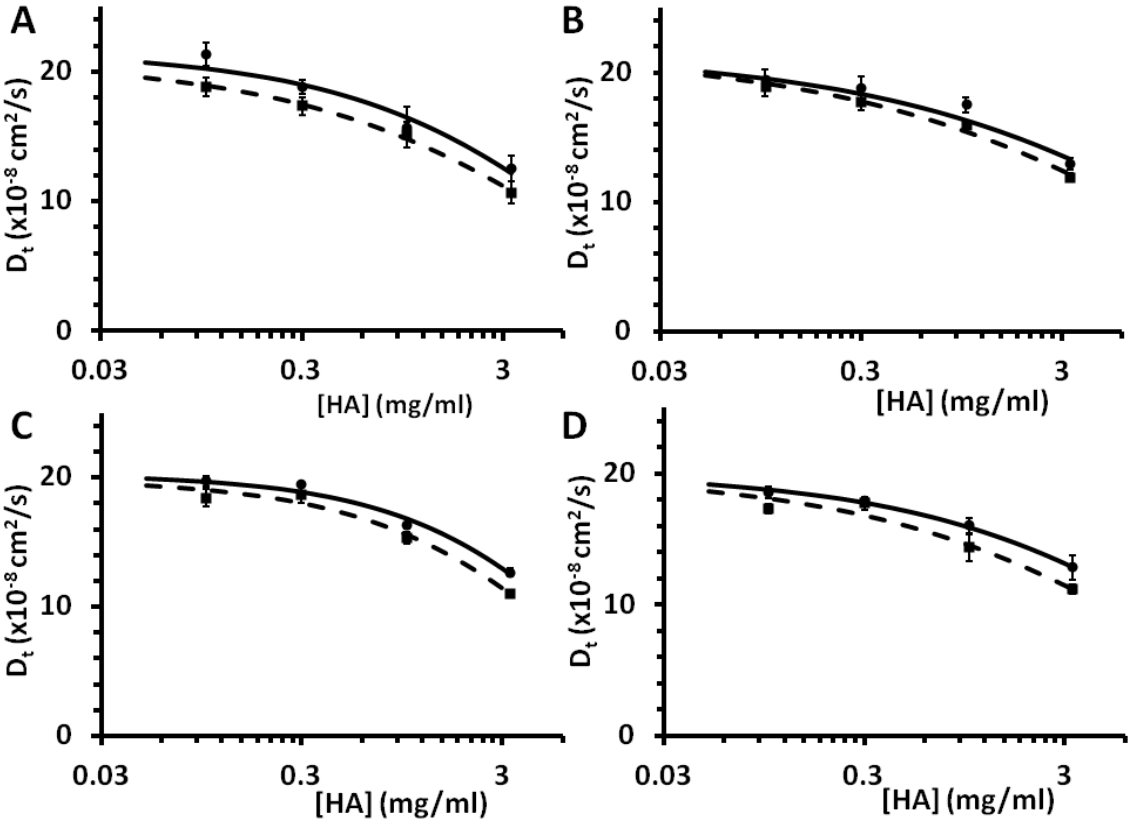

Figure 2-2: Tracer diffusion coefficients of FITC-dextran (2000 kDa) through 1500 kDa HA solutions ± 450µg/ml PRG4 (▪ for HA with PRG4 and ● for HA without PRG4) (**A**), 500 kDa HA solutions ± 450µg/ml PRG4 (**B**); 1500 kDa HA solutions ± 45µg/ml PRG4 (**C**), 500 kDa HA solutions ± 45µg/ml PRG4 (**D**). Data is presented as mean ± SEM (N=4). Data points are fit to the universal scaling equation (dashed lines for HA with PRG4 and solid lines for HA without PRG4).

The addition of PRG4 to the HA solutions caused a decrease in the calculated apparent mesh size, or average pore size, within the HA solution network (**Figure 2-3**). As the concentration of HA in solution is increased, the distance separating each molecule decreased

according to a negative exponential trend. The variation between HA solutions, with and without PRG4, decreases as the solution becomes saturated with HA – at approximately 3.3mg/ml.

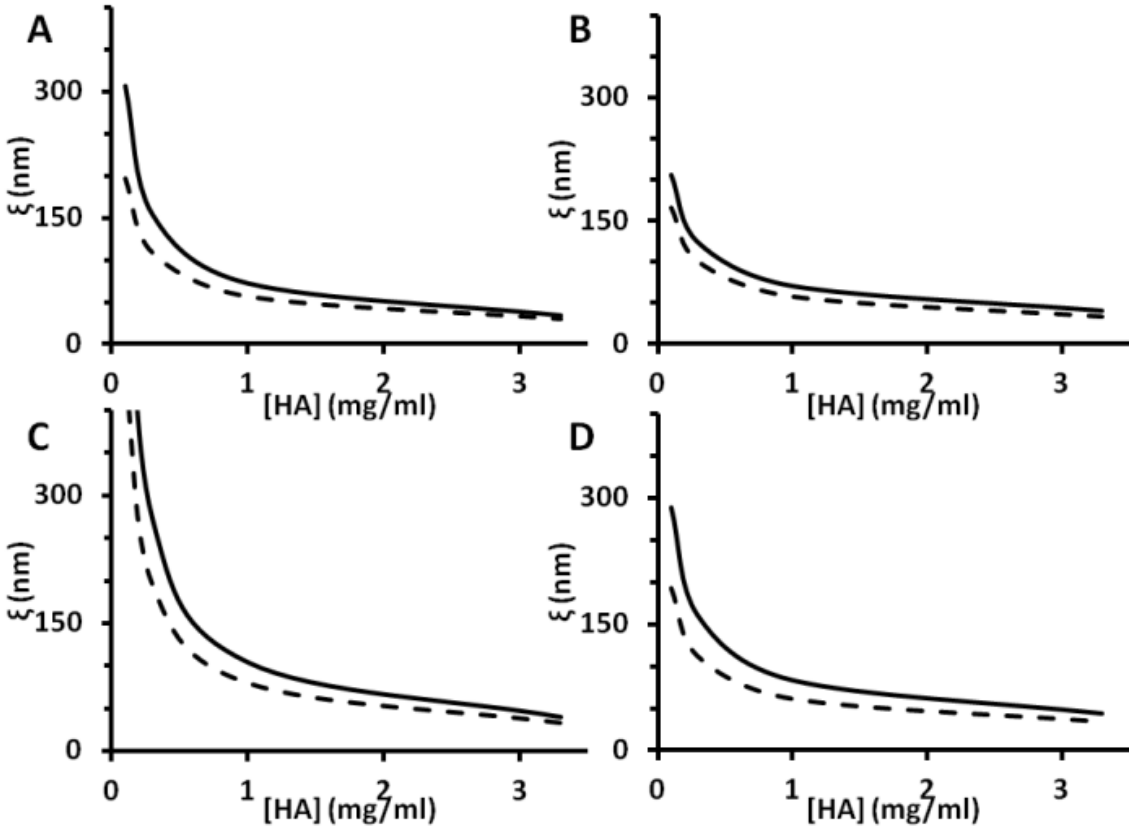

Figure 2-3: Apparent mesh size distribution (ξ) of (**A**) 1500kDa HA ± 450 µg/ml PRG4 , (**B**) 500kDa HA ± 450 µg/ml PRG4; (**C**) 1500kDa HA ± 45 µg/ml PRG4, (**D**) 500kDa HA ± 45 µg/ml PRG4. Dashed lines are used for HA with PRG4 and solid lines for HA without PRG4.

2.4.2 HA±BSA

BSA at 450µg/ml did not slow the diffusion of the FITC-dextran tracer through the HA concentration series, indicating the effect of PRG4 was specific and not a result of a protein being in solution with HA. For 1500kDa HA ± 450µg/ml BSA, the diffusion of the tracer was significantly affected by HA concentration ($p<0.01$) but not the presence of BSA ($p=0.386$), with no interaction effect ($p=0.491$) (**Figure 2-4A**). Similarly for 500kDa HA ± 450µg/ml BSA, the diffusion of the tracer was significantly affected by HA concentration ($p<0.01$) but not the presence of BSA ($p=0.112$), with no interaction effect ($p=1.0$) (**Figure 2-4B**). For all experimental sets there is a clear negative exponential decrease in diffusivity for the tracer as HA concentration increases. The negative exponential trend observed for each increasing HA concentration series (±PRG4) was modeled using the universal scaling equation (**Equation 4**), with a R^2 value of greater than 0.95.The measured D_t^0 for the FITC-dextran tracer was $20.05 \pm 1.36 \times 10^{-8}\, cm^2\, s^{-1}$, and $22.41 \pm 0.83 \times 10^{-8}\, cm^2\, s^{-1}$, for 1500kDa and 500kDa respectively.

No effect of BSA at 45µg/ml on HA solution networks properties was observed either. For 1500kDa HA ± 45µg/ml BSA, the diffusion of the tracer through 1500kDa HA was significantly affected by HA concentration ($p<0.01$) but not the presence of BSA ($p=0.95$), with no interaction effect ($p=0.985$) (**Figure 2-4C**). Similarly for 500kDa HA ± 45µg/ml BSA, the diffusion of the tracer was significantly affected by HA concentration ($p<0.01$) but not the presence of BSA ($p=0.734$), with no interaction effect ($p=0.372$) (**Figure 2-4D**). Also similar to all previous experimental sets, there is a clear negative exponential decrease in diffusivity for the tracer as HA concentration increases which is modeled by the universal scaling equation

(R^2>0.95). The measured D_t^0 for the FITC-dextran tracer was $19.58 \pm 0.77 \times 10^{-8}\, cm^2\, s^{-1}$, and $19.25 \pm 0.96 \times 10^{-8}\, cm^2\, s^{-1}$, for 1500kDa and 500kDa respectively.

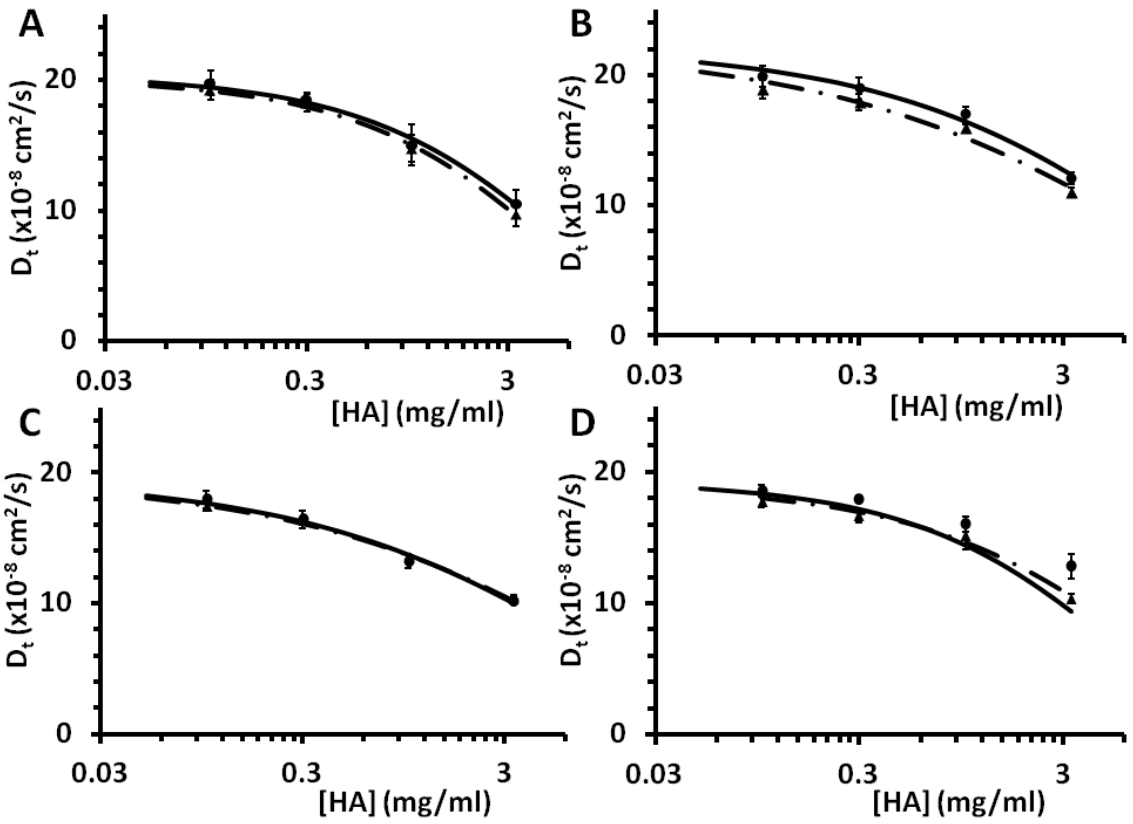

Figure 2-4: Tracer diffusion coefficients of FITC-dextran (2000 kDa) through 1500 kDa HA solutions ± 450µg/ml BSA (Δ for HA with BSA and ● for HA without BSA) (**A**), 500 kDa HA solutions ± 450µg/ml BSA (**B**); 1500 kDa HA solutions ± 45µg/ml BSA (**C**), 500 kDa HA solutions ± 45µg/ml BSA (**D**). Data is presented as mean ± SEM (N=4). Data points are fit to the universal scaling equation (dashed lines for HA with BSA and solid lines for HA without PRG4).

The addition of BSA to the HA solutions did not appear change the calculated average apparent mesh size for each experimental set (**Figure 2-5**).

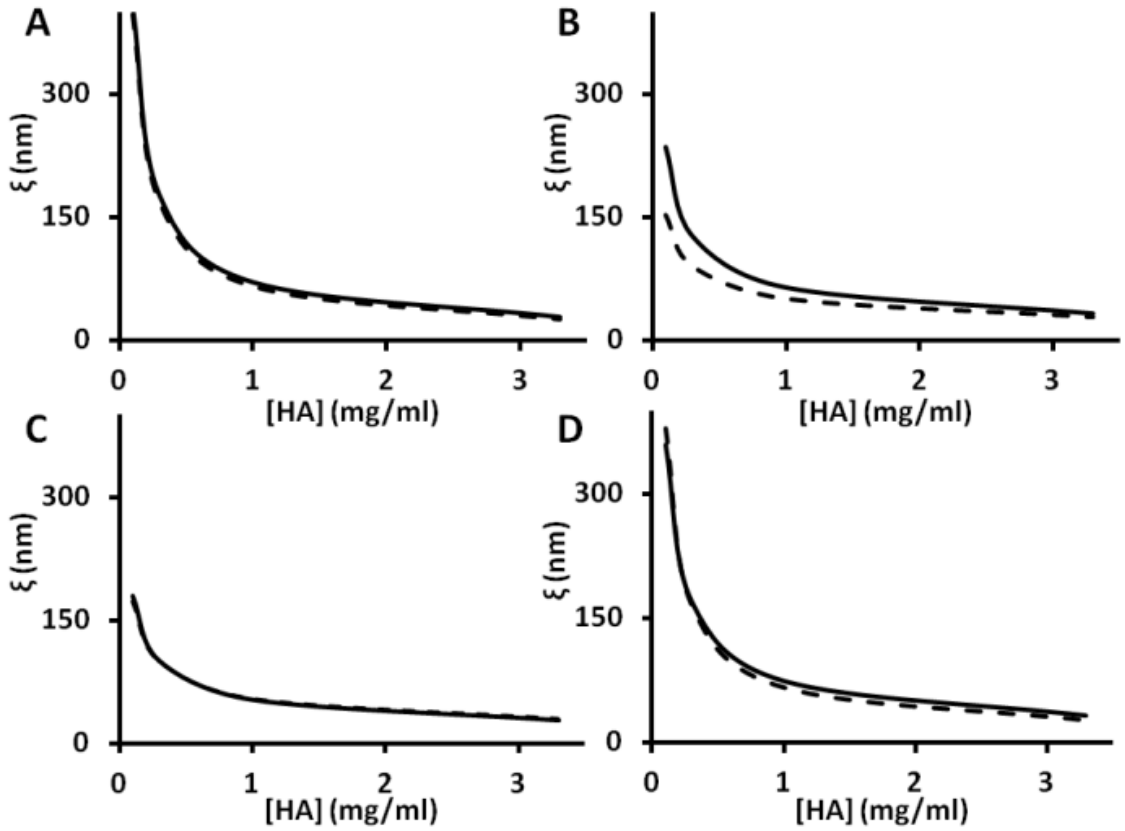

Figure 2-5: Apparent mesh size distribution (ξ) of (A) 1500kDa HA ± 450 µg/ml BSA , (B) 500kDa HA ± 450 µg/ml BSA; (C) 1500kDa HA ± 45 µg/ml BSA, (D) 500kDa HA ± 45 µg/ml BSA. Dashed lines are used for HA with PRG4 and solid lines for HA without PRG4.

2.4.3 HA+PRG4 VS. HA+R/A PRG4

Both PRG4 and R/A PRG4 have a similar effect on the HA solution network. For 1500kDa HA with 450µg/ml of either PRG4 or R/A-PRG4, the diffusion of the tracer was significantly affected by HA concentration ($p<0.01$), but the difference between PRG4 and R/A

PRG4 was not significant (p=0.756), with no interaction effect (p=0.657) (**Figure 2-6A**).The measured D_t^0 for the FITC-dextran tracer for this experimental set was $18.52 \pm 0.82 \times 10^{-8}\, cm^2\, s^{-1}$, . Similarly for PRG4 or R/A-PRG4 at 45μg/ml in 1500kDa HA, the diffusion of the tracer was significantly affected by HA concentration ($p<0.01$), but the difference between PRG4 and R/A PRG4 was not significant (p=0.385), with no interaction effect (p=0.657) (**Figure 2-6B**). The measured D_t^0 for the FITC-dextran tracer for this experimental set was $21.15 \pm 1.13 \times 10^{-8}\, cm^2\, s^{-1}$.

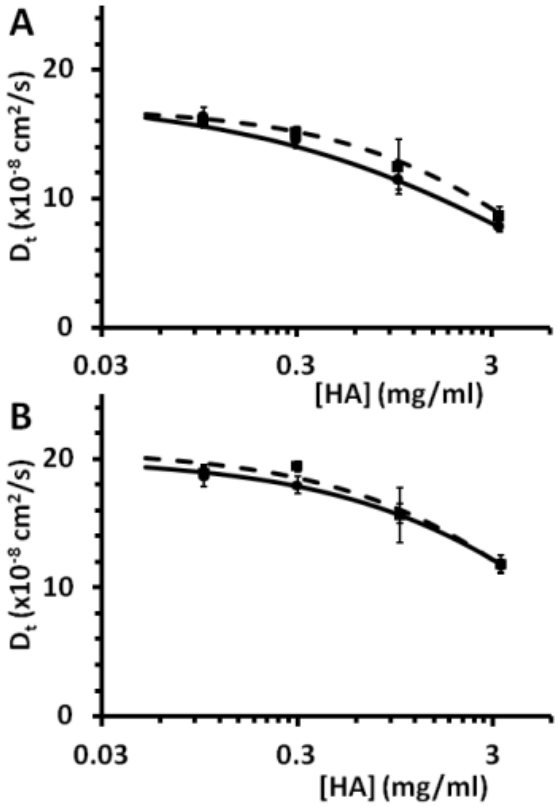

Figure 2-6: Tracer diffusion coefficients of FITC-dextran (2000 kDa) through 1500 kDa HA solutions + 450μg/ml PRG4 or R/A PRG4 (▪ for HA with R/A PRG4 and ● for HA with PRG4).

Data is presented as mean ± SEM (N=4). Data points are fit to the universal scaling equation(dashed lines for HA with R/A PRG4 and solid lines for HA with PRG4).

2.5 DISCUSSION

These results indicate that PRG4, at both physiological (450 μg/ml) and pathological (45 μg/ml) concentrations, can significantly alter the solution properties of 1500 and 500kDa HA. The addition of PRG4 significantly decreased the tracer diffusion at all HA concentrations. All experiments on the HA concentration series of 0 to 3.3mg/ml showed the expected negative exponential trend, which was successfully fit to and modeled by the universal scaling equations. The physical implication of the reduced diffusivity was characterized by the apparent mesh size distribution for each mixture of HA, calculated from the empirical constants (β and ν) from the universal scaling equations, which decreased with the addition of PRG4. PRG4 essentially reduced the permeability of the HA network. This effect was specific to PRG4, and was not seen with the control protein BSA. Interestingly, the reduced permeability caused by PRG4 was not shown to be dependent on its tertiary/quaternary structure as the effect remained after R/A of PRG4.

The HA and PRG4 used in this study are representative of those in native SF and have been used in other studies. The HA MW range used in this study is relevant to both physiological and/or pathophysiological SF, while the explored concentrations cover a larger but encompassing physiological range in order to effectively understand the concentration dependence of HA on network formation[14, 58-60]. The MW of HA used was found to be polydispersed (**Figure 2-1**), yet for the purposes of this study the reported MW was recorded from the supplier. While a large

confocal aperture setting was used, the large NA of the 40x objective lens makes it difficult to assume the system was completely described by 2D diffusion. However, any deviation from a 2D system was assumed to equally effect all samples and have a negligible overall effect on observed trends. No noticeable difference in tracer diffusion between the 1500kDa and 500kDa HA was observed, possibly because of this high polydispersity. Due to the unique properties of PRG4, it was difficult to choose an ideal protein control for the tracer diffusion studies. As such, careful consideration was given to ensure the protein control does not interact with HA. Albumin is physiological abundant within SF, and the interactions of BSA and HA are well understood and known only to be relevant at a low pH[61, 62]. BSA was therefore chosen as a practical and relevant protein control. Measurements for D_t were shown to have a significant variance between experimental sets, with a STD between measured D_t values of $1.4 \times 10^{-8}\, cm^2\, s^{-1}$, To reduce and control for the effect of the natural variations between prepared samples, all comparisons of experimental sets (i.e. one replicate of HA vs. HA+ 450µg/ml PRG4) were performed on the same day from the same prepared HA solutions.

The results from this study agree with those from Gribbon et al.[49] where HA solutions were examined, and extend them to include the effect of PRG4. The results from this study follow a similar trend in regards to the observed effect of HA concentration on FITC-dextran tracer diffusion within a physiological relevant environment[49]. While the results presented here show the same negative exponential trend in tracer diffusion constants in relation to HA concentration, the reported D_t^0 of the 2000kDa FITC-dextran tracer are slightly higher, though still in general agreement. Gribbon et al.[49] measured a D_t^0 for FITC-dextran in PBS of $13.1 \pm 0.5 \times 10^{-8}\, cm^2\, s^{-1}$, which decreases to approximately $7.6 \times 10^{-8}\, cm^2\, s^{-1}$, in 3.3mg/ml of 930kDa HA. This is in comparison to the average measured D_t^0 in our study of

$20.3 \pm 0.4 \times 10^{-8}\, cm^2\, s^{-1},$, which decrease to approximately $11 \times 10^{-8}\, cm^2\, s^{-1},$. Despite this modest difference[49], the D_t^0 for the 2000kDa FITC-dextran tracer calculated here are in agreement with those reported in other studies[63, 64]. The overall differences in D_t^0 for the 2000kDa FITC-dextran tracer reported in literature, including this study, could be related to variations in data analysis and FRAP parameters. Most importantly the high NA of the objective lens suggests that some diffusion is occurring within the Z axis, making the calculated 2D diffusion rates appear larger. Regardless in the variations of recorded D_t^0 the results from this study are in good agreement and therefore validated by previous research. Additionally the results from this study observe the predicted trend in tracer diffusion through increasing HA concentration, and demonstrate a clear and specific effect of PRG4 on HA solution properties.

The mechanism of the PRG4 + HA interaction in solution demonstrated here, and by other supporting studies[2, 30], remains to be completely elucidated. Previously this mechanism has been speculated to be one of physical interaction involving non-covalent entanglements between HA and PRG4 molecules[2]. This interaction is thought to be mediated through the hemopexin (PEX) like and somatomedin B (SMB) like domains on the N- and C-terminus[45, 65], respectively, of PRG4. These regions have been shown to have approximately 60% sequence similarity to somatomedin and/or hemopexin regions, and possibly allow the PRG4 molecule to bind to extracellular matrix[65]. Of particularly note is purified hemopexin's ability to bind to HA, supporting the plausible mechanism for PRG4 entangling HA molecules through this domain[65]. This highly entangled HA matrix is therefore a conceivable explanation for the observed decrease in tracer diffusion and smaller observed mesh sizes when PRG4 is present. In this proposed model PRG4 would bind to HA molecules through cationic regions within the PEX and SMB domains, entangling HA molecules and creating a tighter and more elastic solution

matrix[34]. It is important to state that this model is just one plausible explanation and is yet to be fully validated.

The results demonstrating a similar effect between native PRG4 and R/A PRG4 were somewhat unexpected and may not fit with the above proposed mechanism. The R/A of PRG4 breaks both intra and inter – molecular disulfide bonds, thus reducing PRG4 multimers to monomers, altering tertiary/quaternary structure of the protein, and releasing small protein fragments from the PRG4 molecule[41, 56]. Previously, R/A of PRG4 has been shown to reduce the molecules affinity for the articular cartilage surface[66] through a presumed destruction of globular motifs constituting the lubricin hemopexin-like domain[43]. As such, it was expected here that R/A PRG4 would also lose its ability to alter HA solution properties due to an inability to bind/interact to HA; however this was not observed. There are several possible explanations for this observation, with the first being that R/A may not sufficiently alter the HA binding/interaction sites within the PRG4 molecule. Previously, R/A of human gelatinase was shown not to effect the affinity of gelatines PEX domain to another extracellular molecule, heparin[67]. Another possible explanation is that while PRG4 no longer makes entanglements, it is capable of producing its own solution networks or gels independent of HA. It would then be these PRG4 networks within the space not occupied by HA, and not entanglements with HA, which cause the denser less permeable networks. Formation of gels and networks are well documented in literature on mucins, which relate closely to PRG4 in both structure and function, in which multimers of mucins entangle and interact to create mucus[68]. It is possible that the presence of HA is simply crowding PRG4 molecules into a mucus like, self-assembled network between HA polymer strands. If this were true, it is simply the PRG4 networks occurring in the spaces unoccupied by HA which is impeding the diffusion of the FITC-dextran tracers. Further

support to this phenomena comes from mucin research which has documented that R/A can cause the protein end units to unfold and expose large hydrophobic domains allowing R/A glycoprotein's to aggregate into dense networks[69, 70]. Lastly, an alternative explanation is that both such mechanisms are operative, PRG4 binding to HA and PRG4 networks/self assembly occurring through HA crowding[71], but our FRAP technique is not precise enough to tell the difference between when PRG4 is causing entanglements or simply creating a dense mucin like network of clumped unfolded R/A PRG4. In this case, the similar observed effects of native and R/A PRG4 suggest a limitation of confocal FRAP applied in this way, and provides an opportunity for further exploration in future research. Rheology studies may provide additional insight into the mechanism at work, and the presence of shear force may be able to differentiate the difference between PRG4 mucus networks and interlocking HA networks through PRG4 entanglements[72].

In conclusion, the implications of this study are important to the function of SF within diarthrodial joints. OA patients with diminished PRG4 concentration and altered HA MW distribution within their SF have been shown to have decreased cartilage boundary lubricating ability on the cartilage surface, possibly due to an alteration in how PRG4 and HA interact and provide lubrication[14]. Furthermore, patients suffering from camptodactyl-arthropathy-coxavara-pericarditis (CACP) syndrome, a genetic inability to produce PRG4, suffer from decreased joint lubrication and subsequent degeneration of cartilage. Experiments by Yakubov et al.[73] have demonstrated that boundary lubrication by mucins may be mediated by a complex, stratified layer of adsorbed mucins with the friction at the surface decreasing continuously with an increasing mucin concentration and therefore an increasingly thick mucin layer. Expanding the findings of this study to the cartilage surface suggests that PRG4 might be essential to

organizing HA in a micro layer surrounding the cartilage or ocular surface, similar to the thick "viscous boundary" layer of mucins observed by Yakubov et al.[73]. Future studies will aim at further understanding the role of PRG4 and HA networks, possibly by altering environmental conditions to conform the HA network in predictable ways and change binding site affinity of PRG4[49]. Another opportunity would be using FITC labeled, monodisperse HA in place of a tracer to investigate how the molecules of HA specifically interact with each other in solution when PRG4 is present. Lastly, replicating the experiments from this study with recently available full length recombinant human PRG4[40] and expanding the experimentation to human SF, a more complex HA solution, would be a worthwhile step in exploring the feasibility of potential engineered SF supplements. Collectively, an increased understanding of HA and PRG4 interaction and functional synergism, at the cartilage surface and in solution, would contribute to the understanding of the role altered SF composition plays in OA initiation and progression. These and other findings will hopefully lead to the potential development of new and improved biotherapeutic treatments.

2.6 ACKNOWLEDGEMENTS

This work was supported by the funding from the Natural Science & Engineering Research Council of Canada and the Collaborative Research and Training Experience Program (NSERC-CREATE), the Canadian Arthritis Network, and the Faculty of Kinesiology and Schulich School of Engineering Center for Bioengineering Research and Education at the University of Calgary.

CHAPTER 3: INVESTIGATING THE EFFECT OF RECOMBINANT HUMAN PROTEOGLYCAN 4 ON HYALURONAN SOLUTION PROPERTIES USING CONFOCAL FLUORESCENCE RECOVERY AFTER PHOTOBLEACHING

3.1 ABSTRACT

Objectives: (1) use confocal fluorescence recovery after photobleaching (FRAP) to examine the specific and dose-dependent effect of recombinant human proteoglycan 4 (rhPRG4) on hyaluronan (HA) solution networks by analyzing the diffusion of a FITC-dextran tracer through HA solutions of different molecular weight.

Methods: Confocal FRAP was used to determine the diffusion coefficient of FITC-dextran tracers (D_t) through 1500kDa HA solutions (0 to 3.3mg/ml) ±rhPRG4 at physiological (450μg/ml) or pathophysiological (45μg/ml) concentrations. Empirical constants from fitting data to the universal scaling equation were used to calculate the average distribution of apparent mesh sizes.

Results: The results suggest the presence of rhPRG4, at both physiological and pathological concentrations (450μg/ml and 45μg/ml), causes a significant change in the solution properties of 1500kDa HA. This observed effect is analogous to what was observed from the addition of bovine PRG4 shown in Chapter 2.

Conclusions: These results indicate that rhPRG4, at both physiological and pathological concentrations, can significantly alter the solution properties of HA similar to bovine PRG4. It is suspected that rhPRG4 influences HA through the same mechanism, although still unspecified, as bovine PRG4.

3.2 INTRODUCTION

Synovial fluid (SF), and its constituents hyaluronan (HA) and proteoglycan 4 (PRG4), provide effective lubrication of the articular cartilage surface in synovial joints under physiological loading conditions[8]. Research on the lubricating ability of both PRG4 and HA have demonstrated dose-dependent lubrication on cartilage-cartilage interfaces[8, 30]. More importantly a synergistic relationship between PRG4 and the HA has been observed, which suggests that a PRG4 and HA physical interaction is essential to the observed high lubrication from SF within synovial joints[8, 30]. Previously in Chapter 2, in an attempt to further understand the PRG4 and HA interaction, the effect of PRG4 on HA solution properties was investigated by studying the diffusion of FITC-dextran tracers through HA solution networks using confocal fluorescence recovery after photobleaching (FRAP). It was determined that PRG4 reduces the permeability of the HA solution networks by decreasing the mesh size of the networks. While the exact mechanism remains unknown, the decrease in mesh size was suggested to be a result of either PRG4 and HA physical entanglements or PRG4 networks being formed by the crowding effect of HA[71]. Understanding the exact mechanism of PRG4+HA synergism/interaction, along with other functions of PRG4 in SF, is important because of the necessary roles PRG4 and HA play on the health of SF and lubrication of articular cartilage[15, 74, 75].

The absence of PRG4 has shown to be disastrous to joint health in both humans and mice due to the decreased lubrication and increased wear within the joints[76, 77]. Additionally both PRG4 synthesis within articular joints and PRG4 concentration in SF, has been shown to decrease in animal models of osteoarthritis (OA)[15, 16]. In human OA patients, a subpopulation

of patients containing PRG4 deficient SF was identified[14] indicating that diminished lubrication could be contributing to disease progression in a proportion of OA patients[15, 74, 75]. Furthermore the supplementation of PRG4 into PRG4 deficient SF of OA patients can restore the SFs lubricating ability to healthy levels, suggesting that supplementation with PRG4 may be a viable treatment for OA patients demonstrating diminished lubricating ability[14].

The previously mentioned PRG4 supplementation studies, along with the results from Chapter 2 have a limitation in regards to the source of the PRG4 used. Typically PRG4 has been sourced from bovine SF, or purified media conditioned by bovine cartilage explants, due to its high homology to human PRG4 and ease of production at the lab bench scale[78]. However, the bovine PRG4 used in Chapter 2 has an estimated purity of ~85% with potential co-culturing of similar macromolecules such as fibrinogen[40]. Therefore although bovine PRG4 is appropriate for basic research purposes, potential clinical evaluation of PRG4's efficacy to treat OA, building off the animal models, requires recombinant human protein.

Recently, a full length recombinant human PRG4 (rhPRG4) product was successfully manufactured by Lubris, LLC (Framingham, MA) in partnership with Selexis SA (Geneva, Switzerland) through the insertion of the human PRG4 gene into a Chinese hamster ovary cell line (CHO-M)[40]. This rhPRG4 product has been shown to exhibit immunoreactivity and O-linked glycosylation consistent with that of native PRG4[40]. The product has also been shown to exhibit higher order multimers similar to native PRG4[74]. Most importantly, in addition to rhPRG4's structural congruency to native PRG4, rhPRG4 has been shown to exhibit the same lubricating ability, adhesion to cartilage surface, and cartilage protecting effect as native PRG4[39, 40, 74].

In this Chapter the goal was to assess whether rhPRG4 exhibits similar effects to the solution properties of HA as the native bovine PRG4. Similar to Chapter 2, the objective of this study is to use confocal FRAP to examine the effect of rhPRG4 on HA solution networks by analyzing the diffusion of a FITC-dextran tracer through HA solutions ± PRG4 at 450 μg/ml and 45 μg/ml. Due to the limited difference in results between 1500kDa and 500kDa HA found in Chapter 2, this study will look only at the more physiologically relevant MW of 1500kDa HA.

3.3 MATERIALS AND METHODS

3.3.1 MATERIALS

HA, FITC-dextran and PBS where acquired identically to Chapter 2. rhPRG4 was acquired from Lubris, LLC. The production and characterization of rhPRG4 is summarized in Samsom et al, 2014 (**Figure 3-1**)[40].

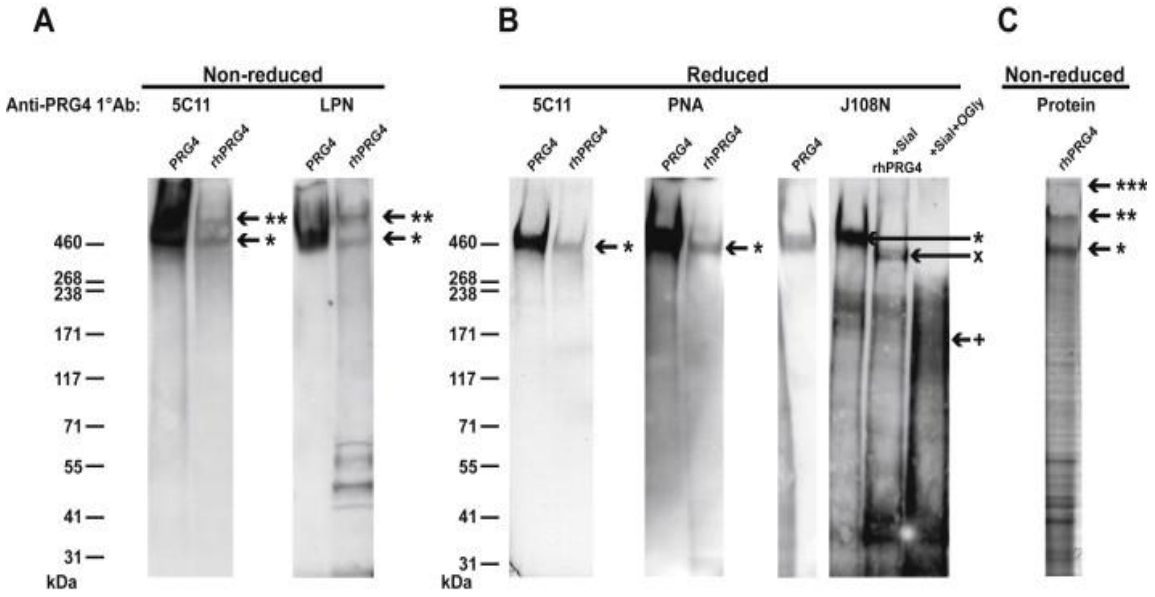

Figure 3-1: SDS-PAGE Western blotting and protein stain, and MS/MS results of recombinant human PRG4 (rhPRG4). SDS-PAGE Western blot analysis of (A) Non-reduced (NR) and (B) R/A PRG4 and rhPRG4 with anti- antibodies LPN, 5C11, J108N, and lectin peanut agglutinin (PNA). SDS-PAGE protein stain of NR rhPRG4 (C).

3.3.2 SAMPLE PREPARATION

Samples were prepared identically to the preparation of HA±PRG4 samples from Chapter 2 with the exception that the PRG4 used is the highly purified recombinant human PRG4 (rhPRG4).

3.3.3 CONFOCAL FRAP PROTOCOL

The confocal FRAP protocol was identical to Chapter 2.

3.3.4 DATA ANALYSIS

The data analysis used was Identical to Chapter 2. All Gaussian time series were fit to a Bessel expansion solution with a R^2 value greater than 0.99.

3.3.5 STATISTICAL METHODS

The statistical analysis used was identical to Chapter 2. In summary an ANOVA was used to assess the effects of both HA concentration and the presence of rhPRG4 at either 450μg/ml or 45μg/ml.

3.4 RESULTS

At 450μg/ml rhPRG4 was shown to slow the diffusion of the FITC-dextran tracer for concentrations of HA, indicating that rhPRG4 has an effect on the HA solution network, analogous to the effect of bovine rhPRG4. For 1500kDa HA ± 450μg/ml PRG4, the diffusion of the tracer was significantly affected by HA concentration ($p<0.01$) and the presence of rhPRG4 ($p<0.05$), with no interaction effect ($p=0.615$) (**Figure 3-2A**). For all experimental sets there was a clear negative exponential decrease in diffusivity for the tracer as HA concentration increases (modeled by the universal scaling equation $R^2>0.95$). The addition of rhPRG4 at 450μg/ml caused an average decrease in D_t of $2.528 \times 10^{-8}\, cm^2\, s^{-1}$. The measured D_t^0 for the FITC-dextran tracer was $22.39 \pm 1.52 \times 10^{-8}\, cm^2\, s^{-1}$.

When rhPRG4 was added at a concentration of 45μg/ml, instead of 450μg/ml, the observed change in HA solution network properties was still evident. For 1500kDa HA ±

45μg/ml rhPRG4, the diffusion of the tracer through was again shown to be significantly affected by HA concentration ($p<0.01$) and the presence of rhPRG4 ($p<0.01$), with no interaction effect ($p=0.235$) (**Figure 3-2B**). Similar to the experimental sets ± 450μg/ml rhPRG4, for all experimental sets there was a clear negative exponential decrease in diffusivity for the tracer as HA concentration increases. The negative exponential trend observed for each increasing HA concentration series (±rhPRG4) was modeled using the universal scaling equation (**Equation 4**), with a R^2 value of greater than 0.95.The addition of rhPRG4 at 45μg/ml in 1500kDa HA caused an average decrease in D_t of $2.08 \times 10^{-8}\, cm^2\, s^{-1}$. The measured D_t^0 for the FITC-dextran tracer was $21.68 \pm 0.60 \times 10^{-8}\, cm^2\, s^{-1}$.

The effect of adding rhPRG4 to the HA solutions can be seen by determining the average apparent mesh size for each experimental set. It is clear in that the addition of rhPRG4 is causing a further decrease in the apparent mesh size, or average pore size within the HA solution network (**Figure 3-3**). As the concentration of HA in solution is increased, the distance separating each molecule is decreased according to a negative exponential trend. This variation between the HA solutions with and without PRG4 begins to decrease as the solution becomes saturated with HA at approximately 3.3mg/ml.

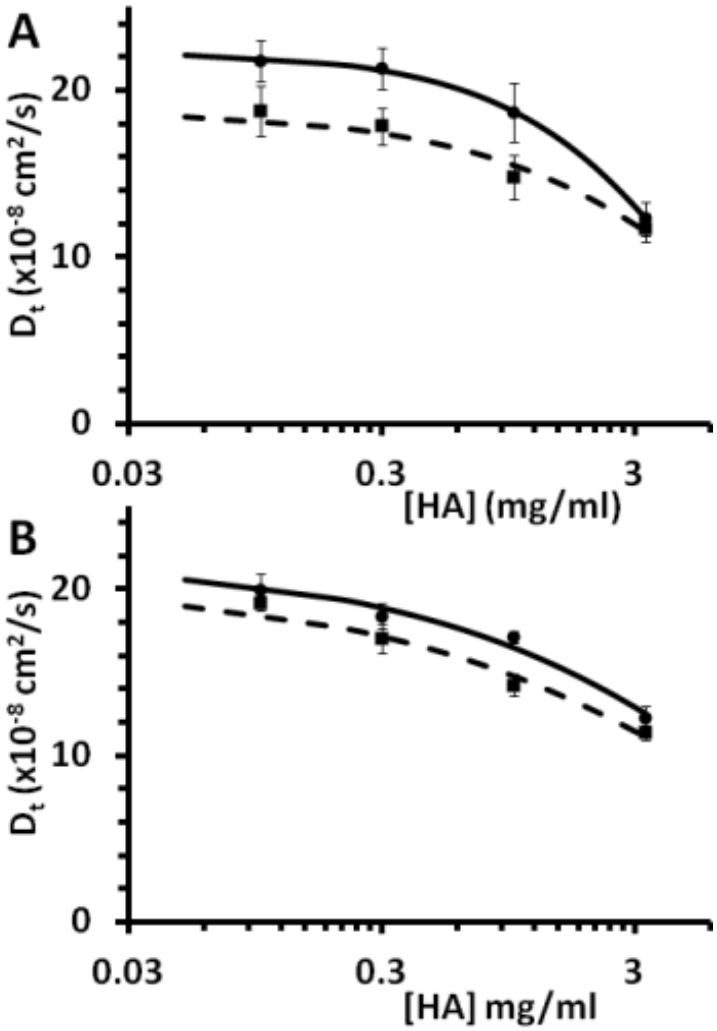

Figure 3-2: Tracer diffusion coefficients of FITC-dextran (2000 kDa) through 1500 kDa HA solutions ± 450µg/ml rhPRG4 (▪ for HA with rhPRG4 and ● for HA without PRG4) (A), 1500 kDa HA solutions ± 45µg/ml rhPRG4 (B). Data is presented as mean ± SEM (N=4). Data points are fit to the universal scaling equation(dashed lines for HA with PRG4 and solid lines for HA without PRG4).

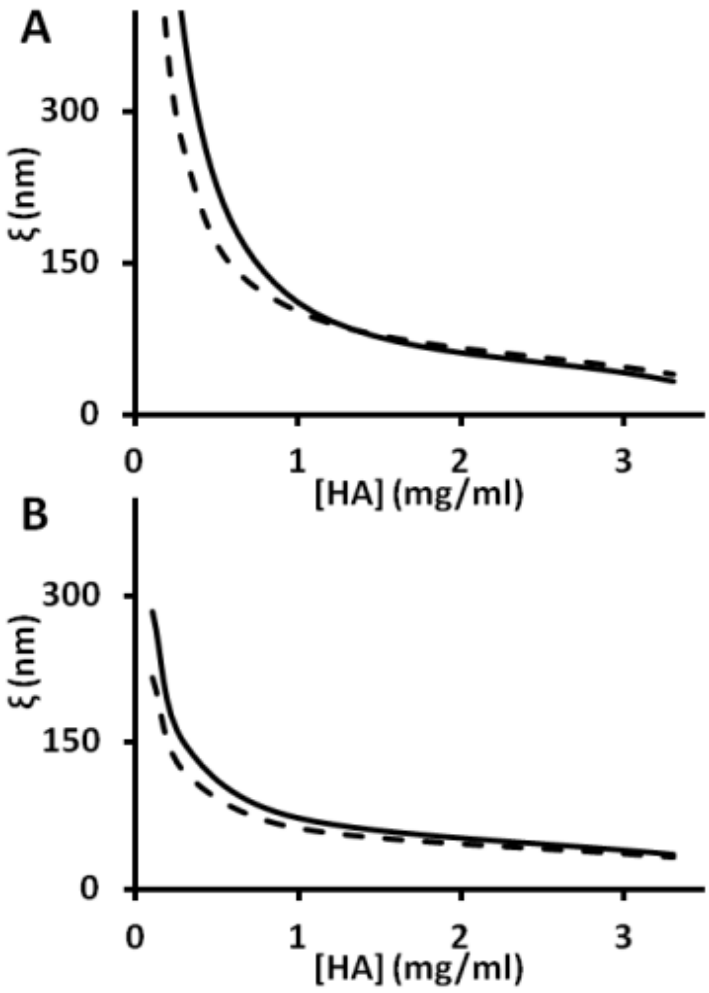

Figure 3-3: Apparent mesh size distribution (ξ) of (**A**) 1500kDa HA ± 450 µg/ml rhPRG4, (**B**) 1500kDa HA ± 45 µg/ml rhPRG4. Dashed lines are used for HA with rhPRG4 and solid lines for HA without rhPRG4.

3.5 DISCUSSION

These results suggest the presence of rhPRG4, at both physiological and pathological concentrations (450μg/ml and 45μg/ml), causes a significant change in the solution properties of 1500kDa HA. This observed effect is analogous to what was observed from the addition of bovine PRG4 shown in Chapter 2. The addition of 450μg/ml and 45μg/ml rhPRG4 caused a decrease in tracer diffusion of $2.528 \times 10^{-8}\, cm^2\, s^{-1}$ and $2.08 \times 10^{-8}\, cm^2\, s^{-1}$ respectively. A negative exponential trend was observed for the diffusion of the tracer though every HA concentration series of 0 to 3.3mg/ml, and this trend was effectively modeled by the universal scaling equation. The mesh size distribution for every measured HA and rhPRG4 mixture was effectively calculated from the empirical constants from the universal scaling equations, β and ν. The calculated apparent mesh size distribution gave an approximate physical representation of the reduced diffusivity of the tracer through HA and rhPRG4 networks, and rhPRG4 was shown to reduce the space between HA molecules.

The limitations of this study are similar to those of Chapter 2. In summary, the rhPRG4 used has been shown to be highly homologous to human PRG4, but still contains lower MW contaminants[40]. The HA used in this study has a MW relevant to physiological MW typically seen in SF, and explored concentrations of HA represent a more encompassing range than typical physiological samples[14, 58-60]. Additionally, in order to reduce experimental error, sample comparisons were performed on the same day from the same prepared HA solution and D_t^0 was kept as a free parameter when fitting experimental sets to the universal scaling equation. Lastly,

the large NA of the 40x objective lens makes it difficult to assume the system was completely described by 2D diffusion. However, any deviation from a 2D system was assumed to equally effect all samples and have a negligible overall effect on observed trends.

As previously suggested, the results from this study agree and extend with those presented in Chapter 2 using bovine PRG4. The range of diffusion coefficients from these experiments also lie within an acceptable range as determined from previous research[49, 63, 64]. Due to the high purity of recombinant PRG4 the results from this study suggest that the results found in Chapter 2 are not a consequence of contaminants co-purified with PRG4 from the bovine explant culture. rhPRG4 is therefore suspected to either form the same crowded networks between HA polymers, or if the effect of PRG4 on HA solution properties is in fact a product of PRG4 entanglements, rhPRG4 contains the same binding domains thought to occur in native PRG4.

The implications of this study are important to the potential eventual development of a PRG4 containing biotherapeutic. Due to the purity, consistency and scale of production needed for a viable commercial product, rhPRG4 is the only practical method of manufacturing a PRG4 biotherapeutic. Recent technological advances have made rhPRG4 a practical reality, although some details of its homology in comparison to native PRG4 need to be explored. The molecule has recently been shown to be structurally similar and function as an effective boundary lubricant: however its behaviour in solution with regards to the viscoelastic nature of SF has yet to be studied. This study provides additional evidence for rhPRG4 homology with native PRG4 in regard to its solution properties, especially with respect to its interaction with HA. The next steps should be to validate the ability of rhPRG4 to change SF chemistry by testing the effect of

rhPRG4 on SF, which is a much more complex solution in comparison to simple HA/PRG4 mixtures.

CHAPTER 4: ASSESSING THE FEASIBILITY OF USING CONFOCAL FRAP TO STUDY SF SAMPLES

4.1 ABSTRACT

Objectives: Assess the feasibility of using confocal fluorescence recovery after photobleaching (FRAP) to study synovial fluid (SF) solution properties by measuring the permeability of normal, pathological, and recombinant human proteoglycan 4 (rhPRG4) supplemented pathological SF samples.

Methods: Confocal FRAP was used to determine the diffusion coefficient of FITC-dextran tracers through SF solutions which have been identified to 1) be sourced from healthy SF and have an average concentration of PRG4; 2) be sourced from OA SF and have a decreased concentration of PRG4; or 3) be sourced from OA SF and have a decreased concentration of PRG4 but supplemented with rhPRG4 to 280μg/ml or 450 μg/ml total PRG4 content.

Results: The permeability of SF samples was successfully determined through the analysis of tracer diffusion as determined by confocal FRAP, although there appeared to be little difference between normal, OA, and supplemented samples.

Conclusions: These results suggest that confocal FRAP can be used to study SF, although the usefulness of the technique is questioned through the lack of difference between OA and normal sample groups. Ultimately a larger and more controlled study is needed to determine the appropriateness of this technique.

4.2 INTRODUCTION

Osteoarthritis (OA) is a disease involving the chronic breakdown of cartilage that effects over 10% or approximately 3 million Canadians, causing pain and significantly decreasing quality of life in patients of the disease[13]. Furthermore, OA is a major cause of long term work disability, and has a major negative impact on the economy[79]. Unfortunately, little is known about the cause, progression and overall biology of the disease[79] and currently OA is primarily treated with therapeutic exercise, pain medication (analgesics and NSAID) and eventually through total joint replacement (TJR) surgery[13]. While TJR is highly effective, the invasive surgery and limited lifespan of artificial joints makes it an unacceptable treatment for younger patients. A better understanding of OA could provide novel and less invasive treatments which combat the disease directly instead of simply treating the symptoms.

Currently OA, and other joint diseases and injuries, are studied through a diverse range of methods including the characterization of composition[80] and lubrication[8, 19] of synovial fluid (SF). It has been found that within OA patients there is a significant variation in the composition of their SF, especially in regards to the lubricating molecules hyaluronan (HA) and proteoglycan 4 (PRG4). Specifically, these studies have shown that many OA SF samples contain low levels of PRG4, and HA with reduced molecular weight (MW)[14, 15, 74, 75]. While these changes in SF composition do not appear in all OA patients, it may represent a sub-population of patients with a similar cause to their OA symptoms. The change in SF composition of these patients was shown to be correlated with a decrease the lubricating ability of the SF possibly contributing to the chronic cartilage damage in the patients[14]. Additionally, while the absence of PRG4 has been shown to significantly alter the viscoelastic properties of SF[2], we

still do not know how the changes in composition from OA can effect solution properties of SF. It could be possible that decreases in PRG4 concentration and HA MW distribution decreases the joints ability to dissipate energy from loads in addition to the alterations in lubrication already observed.

Previously in Chapters 2 and 3 the effect of PRG4, and recombinant human PRG4 (rhPRG4), on solution properties of HA was examined by studying the diffusion of tracers through HA and PRG4 solutions using confocal fluorescence recovery after photobleaching (FRAP). The results of these studies suggested that both bovine and rhPRG4 was capable of altering the solution properties of HA solutions of different concentrations by decreasing the diffusion coefficients of tracers within the solutions. This was determined to be the result of either PRG4 mediated physical entanglements between HA polymers, or HA polymers crowding PRG4 molecules into self aggregating networks. These results, while promising, are driven from HA and PRG4 solutions which are much less complex than the assortment of macromolecules contained within SF. Therefore this study aims at assessing the feasibility of using confocal FRAP to study SF solution properties by measuring the permeability of "normal" (NL), pathological, and rhPRG4 supplemented pathological SF samples.

4.3 MATERIALS AND METHODS

4.3.1 MATERIALS

FITC-dextran and PBS were acquired identically to Chapter 2. rhPRG4 was acquired as stated in Chapter 3[40]. SF was acquired according to previously published methods[14]. In summary, OA SF is aspirated from patients with chronic knee OA patients, prior to therapeutic

treatments. NL SF was obtained through the joint transplantation program of the University of Calgary 4 hours after the death of donors. Both SF samples were clarified via centrifugation (3,000g for 3min at 4C) and stored at -80C with protease inhibitors. The concentration of both PRG4 and HA using respective ELISA tests[14].The lubricating ability of these samples on a cartilage-cartilage interface was tested using well established methods[8]. Acquisition, characterization and lubrication tests were all performed by Dr. Taryn Ludwig (Former PhD student of the Schmidt Lab).

4.3.2 SAMPLE PREPARATION

OA SF samples were identified with lower concentrations of PRG4 and a reduced lubricating ability, and NL SF samples were identified with normal concentrations of PRG4 and lubricating ability. The PRG4 and HA concentrations of all used samples is recorded in **Table 4-1**. Two portions of the OA SF samples was then added to a dried rhPRG4 pellet to increase the total PRG4 concentration in either portion to 280µg/ml or 450µg/ml. 280µg/ml was chosen as a representation of the average healthy SF concentration of PRG4, and 450µg/ml was chosen to represent the upper limit of healthy PRG4 concentration[14]. FITC-dextran was prepared into a concentrated 10mg/ml solution (1xPBS), and added to all SF samples to a final concentration of 0.1mg/ml.

Table 4-1: PRG4 and HA concentration of NL, OA and OA supplemented samples.

	OA SF		**OA SF supplemented to 280µg/ml PRG4**		**OA SF supplemented to 280µg/ml PRG4**		**NL SF**	
	[PRG4] (µg/ml)	**[HA] (mg/ml)**	**[PRG4] (µg/ml)**	**[HA] (mg/ml)**	**[PRG4] (µg/ml)**	**[HA] (mg/ml)**	**[PRG4] (µg/ml)**	**[HA] (mg/ml)**
Mean	146.5	0.642	280 (+133.5 rhPRG4)	0.642	450 (+303.5 rhPRG4)	0.642	265	0.433
STD	56	0.282	N/A	0.282	N/A	0.282	11.5	90.2

4.3.3 CONFOCAL FRAP PROTOCOL

The confocal FRAP protocol was performed identically to Chapter 2.

4.3.4 DATA ANALYSIS

The data analysis used was Identical to Chapter 2. All Gaussian time series were fit to a Bessel expansion solution with a R^2 value greater than 0.99.

4.3.5 STATISTICAL METHODS

Five independent samples of OA SF, from different patients, were analyzed (N=5), and three independent NL SF samples were analyzed (N=3). For each sample, the measured D was a result of 6 averaged confocal FRAP experiments (n=6). All samples were compared with a 1 factor ANOVA.

4.4 RESULTS

The permeability of SF samples was successfully measured through the analysis of tracer diffusion as determined by confocal FRAP, although there appeared to be little difference between NL, OA, and supplemented samples. The D_t values for the OA SF, OA supplemented to 280 µg/ml, OA supplemented to 450 µg/ml, and NL SF groups were $7.23 \pm 1.79 \times 10^{-8}\, cm^2\, s^{-1}$, $7.03 \pm 1.76 \times 10^{-8}\, cm^2\, s^{-1}$, $7.59 \pm 1.87 \times 10^{-8}\, cm^2\, s^{-1}$, $9.69 \pm 1.69 \times 10^{-8}\, cm^2\, s^{-1}$ respectively. It appears from the results that OA SF samples have a decreased tracer diffusion coefficient in comparison to NL SF, although this effect was not significant ($p=0.239$) (Figure 1). The effect of supplementing OA SF with PRG4 had no significant effect. The large SEM found when measuring D_t for each sample group (OA, NL, etc.) indicates a large amount of variation between independent samples, and thus patients, for all sample groups analyzed.

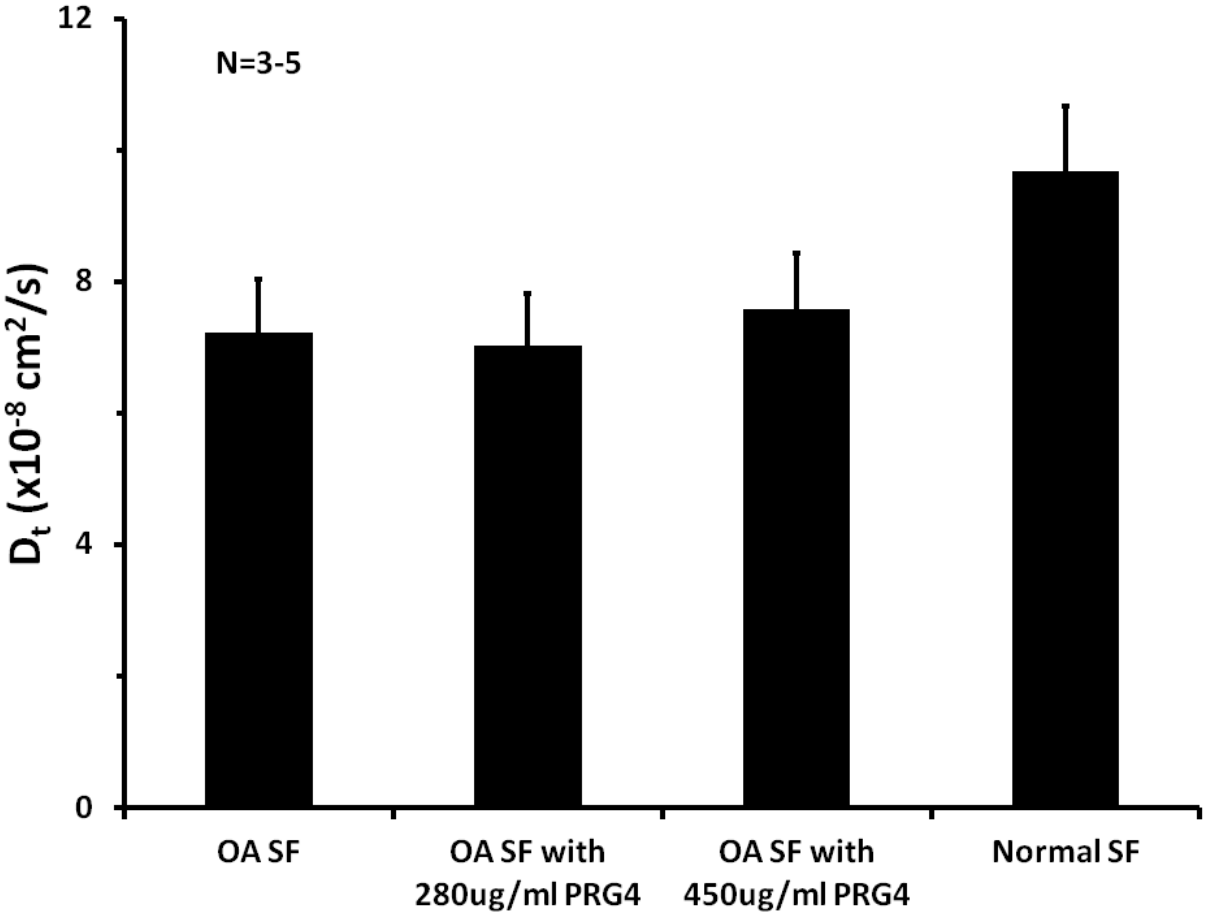

Figure 4-1: Tracer diffusion coefficients of FITC-dextran (2000 kDa) through OA (N=5) SF, OA supplemented to 280 µg/ml (N=5), OA supplemented to 450 µg/ml (N=5), and NL SF samples(N=3). Data is presented as mean ± SEM .

4.5 DISCUSSION

The results suggest that confocal FRAP can be used to investigate the solution properties of SF, although no significant difference was found between samples with different lubricant composition. Despite this lack of significance the confocal FRAP protocol and data analysis procedure worked effectively with SF samples. No auto-fluorescence was observed, and the

tracers were able to move within the solutions and demonstrate a fluorescence recovery. These results validated the use of this technique and demonstrated that the confocal FRAP methods developed for analysis of simple HA/PRG4 solutions can be successfully applied to SF, a highly complicated solution. This experiment gave comparable D values to experiments from Chapter 2 that used similar concentrations of HA and PRG4. The D range of 7.03 to 9.69 $\times 10^{-8}\, cm^2\, s^{-1}$ for SF (PRG4 and HA concentrations in Table 1) compare well to a D of $15.14 \pm 1.01 \times 10^{-8}\, cm^2\, s^{-1}$from Chapter 2 experiments looking at 450 µg/ml PRG4 and 1mg/ml 1500kDa HA. The D values are most likely lower than the controlled 450 µg/ml PRG4 and 1mg/ml 1500kDa HA solution due to SF numerous other components (plasma proteins, glucose, cytokines, etc.[81]) as well as a higher MW distribution of HA.

Despite the lack of significance, **Figure 4-1** suggests the possibility that OA SF is actually less permeable than NL SF. This result is unexpected because OA SF has previously been shown to have reduced viscoelastic properties[82, 83], and it was expected that permeability of the samples would increase. While it is possible some unknown mechanism is at play, this observation is most likely due to the higher relative HA concentrations found in the OA SF samples (**Table 4-1**). Another unexpected result is that supplementation of PRG4 had no observable effect on the permeability of SF samples. This result is contrary to results from Chapters 2 and 3, and provides a great example for the added complexity of SF in comparison to simple HA and PRG4 samples. Both the lowered permeability of OA SF samples in comparison to NL samples and the lack of effect from PRG4 supplementation are also likely a function of the small sample sizes and high variation between SF samples. It is also possible that confocal FRAP is simply unable to detect important differences between the samples, and the technique could be inappropriate for study of SF solution properties. Ultimately, future studies with a larger and

more controlled (less variation between HA concentrations) sample size will provide answers on the appropriateness of this technique.

As discussed above, a limitation of this proof of concept study was low sample size. Due to limited availability of samples, only five OA samples with deficient PRG4 composition and three NL samples with average PRG4 concentration were available for study. The limited availability of samples was due to fact that this study was performed with SF samples that were previously characterized for another study[14], and only a limited amount of characterized samples remained. There was a high amount of variation in the low sample size, and the limited available sample size also resulted in using OA SF samples with higher HA concentration than the NL SF samples. Ideally the HA concentration will be better controlled in future studies. A power analysis for an ANOVA design recommends a sample size of at least 50 when trying to detect a difference with effect size of 2.5.

The primary result of this study is to demonstrate that confocal FRAP can be used to study SF solution properties, although future study with a larger sample size is needed to determine the usefulness of this technique in characterizing and studying SF samples of interest. Ultimately the value of this technique, both as a tool to study SF and potentially as a screening tool to characterize diseased SF, will need to be explored in future studies.

CHAPTER 5: CONCLUSIONS

5.1 SUMMARY OF FINDINGS

The overall goal of this thesis was to use confocal fluorescence recovery after photobleaching (FRAP) to study the synergistic relationship of hyaluronan (HA) and proteoglycan 4 (PRG4) through analyzing the effect of PRG4 on the permeability of HA solutions due to specific interactions between PRG4 and HA polymers in solution. The major findings were:

1) PRG4, at both 45 and 450µg/ml, slowed the diffusion of the FITC-dextran tracer for 500 and 1500kDa HA solutions (0.1, 0.3, 1.0, and 3.3mg/ml) and caused a decrease in the calculated apparent mesh size, or average pore size, within the HA solution network.

2) Recombinant human PRG4 (rhPRG4), at both 45 and 450µg/ml, slowed the diffusion of the FITC-dextran tracer for 1500kDa HA solutions (0.1, 0.3, 1.0, and 3.3mg/ml) and caused a decrease in the calculated apparent mesh size, or average pore size, within the HA solution network.

3) Bovine Serum Albumin (BSA), at both 45 and 450µg/ml, did not slow the diffusion of the FITC-dextran tracer through 500 and 1500kDa HA solutions (0.1, 0.3, 1.0, and 3.3mg/ml), and no change was detected in the calculated apparent mesh size, or average pore size, within the HA solution network.

4) PRG4 as well as reduced and alkylated (R/A) PRG4, at both 45 and 450μg/ml, have a similar effect on 500 and 1500kDa HA solutions (0.1, 0.3, 1.0, and 3.3mg/ml).

5) The permeability of synovial fluid (SF) samples was successfully measured through the analysis of tracer diffusion as determined by confocal FRAP, although there appeared to be little difference between "normal" (NL), osteoarthritic (OA), and supplemented samples.

5.2 DISCUSSION

The studies of this thesis examined the change in solution properties of HA caused by PRG4 in an attempt to understand the concentration and molecular weight (MW) dependence of an HA and PRG4 interaction. An advanced understanding of this PRG4-HA interaction adds to elucidating the mechanism of both the viscoelastic and lubricating properties of SF; though interactions of macromolecules need not be the same at a surface and in solution. Ultimately the results of this study support the theory of an HA and PRG4 viscous boundary layer[73] being formed. This theory suggests that instead of a classical one molecule thick boundary layer, HA and PRG4 organize into a gel which coats the surface of articular cartilage and provides lubrication proportional to the solution properties of this microlayer[73]. The exact mechanism of the formation of this boundary layer requires additional research.

PRG4 was shown to have a universal effect on all concentrations of HA solutions. Additionally, this effect was present at both physiological and pathophysiological concentrations of PRG4. This effect was also observed with rhPRG4 of a high purity suggesting that the change

in HA solution permeability is not a result of contaminants co-purifying with the bovine PRG4 preparation, such as fibrinogen[40]. The observed effect of rhPRG4 also suggests that the recombinant product is capable of performing the same physical interaction in solution that is suspected to occur between bovine PRG4 and HA, or at least resulted in the same observed effects as assessed by confocal FRAP.

For all FRAP experiments performed, the diffusion of fluorophores was modeled as strictly 2D. It has been shown that assuming strictly 2D diffusion is appropriate when using a NA lens, and a large confocal aperture setting[57]. While a large confocal aperture setting was used, the large NA of the 40x objective lens makes it difficult to assume the system is completely described by 2D diffusion. However, any deviation from a 2D system was assumed to equally effect all samples and have a negligible overall effect on observed trends.

The effect of PRG4 was shown to decrease the pore size within the HA networks. This effect may be important to the function of HA+PRG4 networks in solution as well as on the surface of articular cartilage. The decrease in apparent mesh size distribution indicates that PRG4 may alter how the HA network allows molecules, such as nutrients and cytokines, to pass through SF. This could have important implications in regards to residency time of drugs injected into SF, protection of the articular cartilage surface, and diffusion of nutrients to cells within the synovium.

The addition of BSA to HA solutions as a control protein did not replicate results from the addition of PRG4. While BSA has some limitations associated with its use as a control protein, including a smaller specific viscosity in comparison to PRG4, we would have expected some sort of observed effect if the decrease in permeability of HA solutions by PRG4 is simply a result of increased bulk viscosity of the fluid. Therefore, the lack of a significant effect from

BSA suggests that the change caused by PRG4 is a specific interactions between the HA and PRG4 molecule. This specific interaction is thought to be through one, or a combination, of the following proposed mechanisms. The effect of PRG4 may be due to PRG4 physically entangling HA molecules through interactions between HA and PRG4 hemopexin domains, or could be caused by HA crowding PRG4 molecules into a self-assembled network impeding the diffusion of the FITC-dextran tracers. The presence of a non-covalent entanglement occurring between HA and PRG4 is supported by numerous published studies[2, 30, 84], which aim to observe a HA+PRG4 interaction from multiple experimental methods. It has been shown that PRG4 alters the mechanical properties of SF through MPTM studies[2], and the addition of PRG4 alters the rheological behavior of HA solutions[84]. Rheology testing using a Nova rotational rheometer with 40mm parallel plate fixtures has shown that the addition of PRG4 to HA solutions of either 0.3 or 1.0mg/ml increased the solutions viscosity, while the addition of PRG4 to HA solutions of 3.3mg/ml decreased viscosity[84], These mechanical changes to SF are an indicator that the change in solution properties is due to a PRG4 entangled HA matrix because the altered behavior of HA under stress.

The results from comparing the effect of R/A PRG4 and PRG4 suggest, counter to the formerly discussed results, that the mechanism of PRG4-HA interaction in solution is not from a specific physical interaction. The presence of a specific interaction is questioned because the proposed binding sites should be destroyed or altered through the reduction of disulphide bridges present within the protein domains on the terminal ends of the PRG4 molecule[43]. However, the R/A of PRG4 could result in the exposure of large hydrophobic domains within the protein, potentially causing the R/A PRG4 to aggregate through interaction of these hydrophobic domains; such a phenomena has been observed with mucins[70]. Such aggregates in spaces not

occupied by HA could still result in the slowed diffusion of the FITC-tracers, resulting in a similar observed or measured effect. As such, it is possible that confocal FRAP cannot distinguish between alterations in solution properties caused by these R/A PRG4 aggregates and the entangled PRG4/HA network. Therefore, this presents a limitation of the confocal FRAP technique in this regard, and provides an opportunity for future study with other techniques to examine the effect of physiological PRG4 structure (e.g. non-reduced monomeric vs. multimeric forms[85]) on HA solution properties. Interestingly, rheological studies on HA and R/A PRG4 show that R/A PRG4 is unable to change the viscosity of HA solutions[84]. This provides further evidence that while R/A PRG4 may delay diffusion of tracers, this is not due to the same mechanism that is displayed by unaltered PRG4.

In the last part of this thesis confocal FRAP was used in a pilot study to examine human SF samples of interest, which are significantly more complicated than simple HA and PRG4 solutions. The permeability of the SF samples of interested, which included those with altered PRG4 content, was successfully determined through the analysis of tracer diffusion as determined by confocal FRAP. This was a significant finding as there were potential concerns with auto-fluorescence and/or lack of diffusion with the human SF samples. However, there appeared to be little difference between normal, OA (and PRG4 deficient), and supplemented samples. These results suggest that confocal FRAP can be used to study the solution properties of SF, although a larger and more controlled study is needed to truly assess the usefulness of confocal FRAP in assessing and examining the macromolecular composition – function relationship in normal and OA human SF.

This thesis is the first to use confocal FRAP to study how PRG4 and HA interact synergistically within solution. The results presented contribute to the overall understanding of

SF physiology, which has previously been studied from a rheological and tribological perspective. Combining insights from studying HA/PRG4 solution properties through confocal FRAP, with present and future rheology and friction studies will result in a more thorough standing of each field of study independently, and as a complete system. The clinical value of the results of this study, as presented currently remains to be determined, but they provide a framework for an advanced understanding of both SF physiology and pathology.

5.3 FUTURE WORK

The results from this thesis, and establishment of a method, provide the framework for follow up studies and future work. Specifically, while this study investigates the HA concentration and MW impact of a PRG4-HA interaction in solution, it does little to elucidate the exact mechanism of interaction occurring between HA and PRG4. As such, future studies could continue to use FRAP to analyze the effect of changing environmental conditions such as pH and salt concentration, and therefore HA conformation[49], on PRG4 and HA solution properties. Additionally, Ca^{2+} has been shown to block binding sites and alter binding site affinity in fibrinogen. Due to the structural similarity between fibrinogen and PRG4, altering the environmental concentration of Ca^{2+} could be a valuable tool in distinguishing between whether PRG4 is actually creating entanglements, or simply being crowded into a network.

A significant advantage of confocal FRAP over other solution probing techniques is its ability to observe the diffusion of any fluorescently labeled molecule. Using FITC labelled, monodisperse, HA molecules in place of dextran tracers could give more information in regard

to how HA interacts with HA or HA-PRG4 networks. Studying the self diffusion of HA would therefore be a valuable future goal.

A significant limitation of the proposed study was the assumption of a strictly 2D diffusing system. This 2D assumption is appropriate when using a NA lens, and a large confocal aperture setting[57], but in the presented studies a large NA 40x objective lens was used. The use of a 40x lens was used to get a more defined bleaching area, but its use makes it difficult to assume the system is completely described by 2D diffusion. It was assumed that any deviation from a 2D system equally effect all samples and had a negligible overall effect on observed trends. For future studies, a 3D model should be used to fit data and provide more accurate absolute value for the diffusion of the FITC-dextran tracer.

Finally, future work should aim at using confocal FRAP to study a large population of human SF samples, both normal and OA, and assess whether this technique can provide meaningful results. Such work could answer whether confocal FRAP could be used as another tool to study SF and potentially eventually as a screening tool for altered macromolecular composition-function in SF and therefore identifying diseased SF.

CHAPTER 6: REFERENCES

1. Zappone, B., et al., *Molecular aspects of boundary lubrication by human lubricin: Effect of disulfide bonds and enzymatic digestion.* Langmuir, 2008. **24**(4): p. 1495-1508.
2. Jay, G., et al., *The role of lubricin in the mechanical behavior of synovial fluid.* Proceedings of the National Academy of Sciences, 2007. **104**(15): p. 6194-6199.
3. Ateshian, G.A., *The role of interstitial fluid pressurization in articular cartilage lubrication.* Journal of biomechanics, 2009. **42**(9): p. 1163-1176.
4. Chan, S., et al., *The role of lubricant entrapment at biological interfaces: Reduction of friction and adhesion in articular cartilage.* Journal of biomechanics, 2011. **44**(11): p. 2015-2020.
5. Coles, J.M., D.P. Chang, and S. Zauscher, *Molecular mechanisms of aqueous boundary lubrication by mucinous glycoproteins.* Current Opinion in Colloid & Interface Science, 2010. **15**(6): p. 406-416.
6. Caligaris, M. and G.A. Ateshian, *Effects of sustained interstitial fluid pressurization under migrating contact area, and boundary lubrication by synovial fluid, on cartilage friction.* Osteoarthritis and Cartilage, 2008. **16**(10): p. 1220-1227.
7. Hills, B., *Boundary lubrication in vivo.* Proceedings of the Institution of Mechanical Engineers, Part H: Journal of Engineering in Medicine, 2000. **214**(1): p. 83-94.
8. Schmidt, T.A., et al., *Boundary lubrication of articular cartilage: Role of synovial fluid constituents.* Arthritis & Rheumatism, 2007. **56**(3): p. 882-891.
9. Radin, E.L. and I.L. Paul, *Does cartilage compliance reduce skeletal impact loads?. the relative force-attenuating properties of articular cartilage, synovial fluid, periarticular soft tissues and bone.* Arthritis & Rheumatism, 1970. **13**(2): p. 139-144.
10. Balazs, E.A., *The Physical Properties of Synovial Fluid and the Special Role~ oi Hyaluronic Acid.* Disorders of the Knee, JB LippincoU Co., Philadelphia, 1974: p. 63-75.
11. Oates, K.M.N., et al., *Rheopexy of synovial fluid and protein aggregation.* Journal of The Royal Society Interface, 2006. **3**(6): p. 167-174.
12. Schurz, J., *Rheology of synovial fluids and substitute polymers.* Journal of Macromolecular Science, Part A: Pure and Applied Chemistry, 1996. **33**(9): p. 1249-1262.
13. *Osteoarthritis*. 2014 [cited 2014 June]; Available from: http://www.arthritis.ca/page.aspx?pid=941.
14. Ludwig, T.E., et al., *Diminished cartilage-lubricating ability of human osteoarthritic synovial fluid deficient in proteoglycan 4: Restoration through proteoglycan 4 supplementation.* Arthritis & Rheumatism, 2012. **64**(12): p. 3963-3971.
15. Teeple, E., et al., *Coefficients of friction, lubricin, and cartilage damage in the anterior cruciate ligament-deficient guinea pig knee.* Journal of Orthopaedic Research, 2008. **26**(2): p. 231-237.
16. Young, A.A., et al., *Proteoglycan 4 downregulation in a sheep meniscectomy model of early osteoarthritis.* Arthritis Research and Therapy, 2006. **8**(2): p. R41.
17. Wei, L., et al., *Comparison of differential biomarkers of osteoarthritis with and without posttraumatic injury in the Hartley guinea pig model.* Journal of Orthopaedic Research, 2010. **28**(7): p. 900-906.

18. Neu, C., et al., *Increased friction coefficient and superficial zone protein expression in patients with advanced osteoarthritis.* Arthritis & Rheumatism, 2010. **62**(9): p. 2680-2687.
19. Ballard, B.L., et al., *Effect of tibial plateau fracture on lubrication function and composition of synovial fluid.* The Journal of Bone & Joint Surgery, 2012. **94**(10): p. e64 1-9.
20. Benz, M., N. Chen, and J. Israelachvili, *Lubrication and wear properties of grafted polyelectrolytes, hyaluronan and hylan, measured in the surface forces apparatus.* Journal of Biomedical Materials Research Part A, 2004. **71**(1): p. 6-15.
21. Moskalewski, S. and E. Jankowska-Steifer, *Hydrostatic and boundary lubrication of joints--nature of boundary lubricant.* Ortopedia, traumatologia, rehabilitacja, 2012. **14**(1): p. 13.
22. Cowman, M.K. and S. Matsuoka, *Experimental approaches to hyaluronan structure.* Carbohydrate research, 2005. **340**(5): p. 791-809.
23. Laurent, T.C., *An early look at macromolecular crowding.* Biophys Chem, 1995. **57**(1): p. 7-14.
24. Laurent, T. and A. Ogston, *The interaction between polysaccharides and other macromolecules. 4. The osmotic pressure of mixtures of serum albumin and hyaluronic acid.* Biochemical Journal, 1963. **89**(2): p. 249.
25. Spagnoli, C., et al., *Hyaluronan conformations on surfaces: effect of surface charge and hydrophobicity.* Carbohydrate research, 2005. **340**(5): p. 929-941.
26. Dunn, A.C., W.G. Sawyer, and T.E. Angelini, *Gemini Interfaces in Aqueous Lubrication with Hydrogels.* Tribology Letters, 2014. **54**(1): p. 59-66.
27. Jay, G.D., K. Haberstroh, and C.J. Cha, *Comparison of the boundary-lubricating ability of bovine synovial fluid, lubricin, and Healon.* Journal of biomedical materials research, 1998. **40**(3): p. 414-418.
28. Chan, S.M.T., et al., *Atomic force microscope investigation of the boundary-lubricant layer in articular cartilage.* Osteoarthritis and Cartilage, 2010. **18**(7): p. 956-963.
29. Shi, L., et al., *Friction coefficients for mechanically damaged bovine articular cartilage.* Biotechnology and bioengineering, 2012. **109**(7): p. 1769-1778.
30. Kwiecinski, J., et al., *The effect of molecular weight on hyaluronan's cartilage boundary lubricating ability–alone and in combination with proteoglycan 4.* Osteoarthritis and Cartilage, 2011. **19**(11): p. 1356-1362.
31. Gigante, A. and L. Callegari, *The role of intra-articular hyaluronan (Sinovial®) in the treatment of osteoarthritis.* Rheumatology international, 2011. **31**(4): p. 427-444.
32. Schumacher, B., et al., *A novel proteoglycan synthesized and secreted by chondrocytes of the superficial zone of articular cartilage.* Archives of biochemistry and biophysics, 1994. **311**(1): p. 144-152.
33. JAY, G.D., D.E. BRITT, and C.-J. Cha, *Lubricin is a product of megakaryocyte stimulating factor gene expression by human synovial fibroblasts.* Journal of rheumatology, 2000. **27**(3): p. 594-600.
34. Jay, G.D., et al., *Homology of lubricin and superficial zone protein (SZP): products of megakaryocyte stimulating factor (MSF) gene expression by human synovial fibroblasts and articular chondrocytes localized to chromosome 1q25.* Journal of Orthopaedic Research, 2001. **19**(4): p. 677-687.

35. Steele, B.L., M.C. Alvarez-Veronesi, and T.A. Schmidt, *Molecular weight characterization of PRG4 proteins using multi-angle laser light scattering (MALLS).* Osteoarthritis and Cartilage, 2012.
36. Marin, F., et al., *Molluscan shell proteins: primary structure, origin, and evolution.* Current topics in developmental biology, 2007. **80**: p. 209-276.
37. Swann, D.A., H.S. Slayter, and F.H. Silver, *The molecular structure of lubricating glycoprotein-I, the boundary lubricant for articular cartilage.* Journal of Biological Chemistry, 1981. **256**(11): p. 5921-5925.
38. Chang, D.P., et al., *Conformational Mechanics, Adsorption, and Normal Force Interactions of Lubricin and Hyaluronic Acid on Model Surfaces†.* Langmuir, 2008. **24**(4): p. 1183-1193.
39. Gleghorn, J.P., et al., *Boundary mode lubrication of articular cartilage by recombinant human lubricin.* Journal of Orthopaedic Research, 2009. **27**(6): p. 771-777.
40. Samsom, M.L., et al., *Characterization of Full-Length Recombinant Human Proteoglycan 4 as an Ocular Surface Boundary Lubricant.* Experimental Eye Research, (0).
41. Schmidt, T.A., A.H. Plaas, and J.D. Sandy, *Disulfide-bonded multimers of proteoglycan 4 (PRG4) are present in normal synovial fluids.* Biochimica et Biophysica Acta (BBA)-General Subjects, 2009. **1790**(5): p. 375-384.
42. Flannery, C.R., et al., *Prevention of cartilage degeneration in a rat model of osteoarthritis by intraarticular treatment with recombinant lubricin.* Arthritis & Rheumatism, 2009. **60**(3): p. 840-847.
43. Jones, A.R., et al., *Binding and localization of recombinant lubricin to articular cartilage surfaces.* Journal of orthopaedic research, 2007. **25**(3): p. 283-292.
44. Swann, D., et al., *Role of hyaluronic acid in joint lubrication.* Annals of the rheumatic diseases, 1974. **33**(4): p. 318.
45. Jay, G.D., D.A. Harris, and C.-J. Cha, *Boundary lubrication by lubricin is mediated by O-linked β (1-3) Gal-GalNAc oligosaccharides.* Glycoconjugate journal, 2001. **18**(10): p. 807-815.
46. Kappler, J., et al., *Single-molecule imaging of hyaluronan in human synovial fluid.* Journal of biomedical optics, 2010. **15**(6): p. 060504-060504-3.
47. Axelrod, D., et al., *Mobility measurement by analysis of fluorescence photobleaching recovery kinetics.* Biophysical journal, 1976. **16**(9): p. 1055-1069.
48. Kubitscheck, U., P. Wedekind, and R. Peters, *Lateral diffusion measurement at high spatial resolution by scanning microphotolysis in a confocal microscope.* Biophysical journal, 1994. **67**(3): p. 948-956.
49. Gribbon, P., B.C. Heng, and T.E. Hardingham, *The molecular basis of the solution properties of hyaluronan investigated by confocal fluorescence recovery after photobleaching.* Biophysical journal, 1999. **77**(4): p. 2210-2216.
50. Carslaw, H. and J. Jaeger, *Some two-dimensional problems in conduction of heat with circular symmetry.* Proceedings of the London mathematical society, 1940. **2**(1): p. 361-388.
51. Phillies, G.D., *The hydrodynamic scaling model for polymer self-diffusion.* The Journal of Physical Chemistry, 1989. **93**(13): p. 5029-5039.

52. De Smedt, S.C., et al., *Structural information on hyaluronic acid solutions as studied by probe diffusion experiments.* Macromolecules, 1994. **27**(1): p. 141-146.
53. Lee, H.G. and M.K. Cowman, *An agarose gel electrophoretic method for analysis of hyaluronan molecular weight distribution.* Anal Biochem, 1994. **219**(2): p. 278-87.
54. Steele, B., M. Alvarez-Veronesi, and T. Schmidt, *Molecular weight characterization of PRG4 proteins using multi-angle laser light scattering (MALLS).* Osteoarthritis and Cartilage, 2013. **21**(3): p. 498-504.
55. Swann, D.A., et al., *The lubricating activity of synovial fluid glycoproteins.* Arthritis & Rheumatism, 1981. **24**(1): p. 22-30.
56. Rhee, D.K., et al., *Consequences of disease-causing mutations on lubricin protein synthesis, secretion, and post-translational processing.* Journal of Biological Chemistry, 2005. **280**(35): p. 31325-31332.
57. Gribbon, P. and T.E. Hardingham, *Macromolecular diffusion of biological polymers measured by confocal fluorescence recovery after photobleaching.* Biophysical journal, 1998. **75**(2): p. 1032-1039.
58. Dahl, L., et al., *Concentration and molecular weight of sodium hyaluronate in synovial fluid from patients with rheumatoid arthritis and other arthropathies.* Annals of the rheumatic diseases, 1985. **44**(12): p. 817-822.
59. Laurent, T.C., M. Ryan, and A. Pietruszkiewicz, *Fractionation of hyaluronic acid the polydispersity of hyaluronic acid from the bovine vitreous body.* Biochimica et biophysica acta, 1960. **42**: p. 476-485.
60. Fraser, J., T. Laurent, and U. Laurent, *Hyaluronan: its nature, distribution, functions and turnover.* Journal of internal medicine, 1997. **242**(1): p. 27-33.
61. Xu, S., et al., *Characteristics of complexes composed of sodium hyaluronate and bovine serum albumin.* CHEMICAL AND PHARMACEUTICAL BULLETIN-TOKYO-, 2000. **48**(6): p. 779-783.
62. Lenormand, H., et al., *The hyaluronan–protein complexes at low ionic strength: How the hyaluronidase activity is controlled by the bovine serum albumin.* Matrix Biology, 2009. **28**(6): p. 365-372.
63. Peters, R., *Nucleo-cytoplasmic flux and intracellular mobility in single hepatocytes measured by fluorescence microphotolysis.* The EMBO journal, 1984. **3**(8): p. 1831.
64. Poitevin, E. and P. Wahl, *Study of the translational diffusion of macromolecules in beads of gel chromatography by the FRAP method.* Biophysical chemistry, 1988. **31**(3): p. 247-258.
65. Bao, J.-p., W.-p. Chen, and L.-d. Wu, *Lubricin: a novel potential biotherapeutic approaches for the treatment of osteoarthritis.* Molecular biology reports, 2011. **38**(5): p. 2879-2885.
66. Nugent-Derfus, G., et al., *PRG4 exchange between the articular cartilage surface and synovial fluid.* Journal of Orthopaedic Research, 2007. **25**(10): p. 1269-1276.
67. Wallon, U.M. and C.M. Overall, *The Hemopexin-like Domain (C Domain) of Human Gelatinase A (Matrix Metalloproteinase-2) Requires Ca2+ for Fibronectin and Heparin Binding BINDING PROPERTIES OF RECOMBINANT GELATINASE AC DOMAIN TO EXTRACELLULAR MATRIX AND BASEMENT MEMBRANE COMPONENTS.* Journal of Biological Chemistry, 1997. **272**(11): p. 7473-7481.

68. Thornton, D.J. and J.K. Sheehan, *From mucins to mucus: toward a more coherent understanding of this essential barrier.* Proceedings of the American Thoracic Society, 2004. **1**(1): p. 54-61.
69. Shankar, V., et al., *Evidence of hydrophobic domains in human respiratory mucins. Effect of sodium chloride on hydrophobic binding properties.* Biochemistry, 1990. **29**(24): p. 5856-5864.
70. Davies, J.R., C. Wickström, and D.J. Thornton, *Gel-forming and cell-associated mucins: preparation for structural and functional studies,* in *Mucins*. 2012, Springer. p. 27-47.
71. Mary K.. Cowman, M.H., Jin Ryoun Kim, Han Yuan, and Yang Hu, *Macromolecular Crowding in the Biomatrix", in Structure and Function of Biomatrix: Control of Cell Behavior and Gene Expression.* Matrix Biology Institute, 2012: p. 45-66.
72. Rinaudo, M., *Rheological investigation on hyaluronan–fibrinogen interaction.* International journal of biological macromolecules, 2008. **43**(5): p. 444-450.
73. Yakubov, G.E., et al., *Viscous Boundary Lubrication of Hydrophobic Surfaces by Mucin.* Langmuir, 2009. **25**(4): p. 2313-2321.
74. Jay, G.D., et al., *Prevention of cartilage degeneration and restoration of chondroprotection by lubricin tribosupplementation in the rat following anterior cruciate ligament transection.* Arthritis & Rheumatism, 2010. **62**(8): p. 2382-2391.
75. Elsaid, K., et al., *Decreased lubricin concentrations and markers of joint inflammation in the synovial fluid of patients with anterior cruciate ligament injury.* Arthritis & Rheumatism, 2008. **58**(6): p. 1707-1715.
76. Rhee, D.K., et al., *The secreted glycoprotein lubricin protects cartilage surfaces and inhibits synovial cell overgrowth.* Journal of Clinical Investigation, 2005. **115**(3): p. 622-631.
77. Marcelino, J., et al., *CACP, encoding a secreted proteoglycan, is mutated in camptodactyly-arthropathy-coxa vara-pericarditis syndrome.* Nature genetics, 1999. **23**(3): p. 319-322.
78. Flannery, C.R., et al., *Articular cartilage superficial zone protein (SZP) is homologous to megakaryocyte stimulating factor precursor and is a multifunctional proteoglycan with potential growth-promoting, cytoprotective, and lubricating properties in cartilage metabolism.* Biochemical and biophysical research communications, 1999. **254**(3): p. 535-541.
79. Safety, C.C.f.O.H. *Osteoarthritis*. 2014 [cited 2014; Available from: http://www.ccohs.ca/oshanswers/diseases/osteoart.html.
80. Blewis, M., et al., *A model of synovial fluid lubricant composition in normal and injured joints.* Eur Cell Mater, 2007. **13**: p. 26-39.
81. Lipowitz, A.J., *Synovial Fluid*, in *Textbook of Small Animal Orthopaedics*. 1985.
82. Peyron, J.G., *A new approach to the treatment of osteoarthritis: viscosupplementation.* Osteoarthritis and Cartilage, 1993. **1**(2): p. 85-87.
83. Sun, S.-F., et al., *The effect of three weekly intra-articular injections of hyaluronate on pain, function, and balance in patients with unilateral ankle arthritis.* The Journal of Bone & Joint Surgery, 2011. **93**(18): p. 1720-1726.
84. Ludwig TE, C.M., Schmidt TA, *Effects of Concentration and Structure on PRG4 Viscosity and Interaction with Hyaluronan.* Trans Orthop Res Soc, 2014. **39**(372).

85. Nugent-Derfus, G.E., et al., *PRG4 exchange between the articular cartilage surface and synovial fluid.* Journal of Orthopaedic Research, 2007. **25**(10): p. 1269-1276.

APPENDIX A: MATLAB® ANALYSIS PROGRAM (WRITTEN BY MICHAEL SAMSOM)

A.1. Image Generator (convert, scale and filter .lsm FRAP files to Microsoft access table shortcut for easy analysis)

```
%%
%
% AUTHOR: Michael Samsom
% DATE: June 2013 (version 1.2)
% DESCRIPTION: This is the main module of the image analysis program.
% FUNCTIONS CALLED:
% LSMreader
% imProcessor2



clear all; close all; clc;


% VARIABLES-
%--------------------------------------------------------------------------
pn = uigetdir('C:\Users'); % get path from user
% pn='C:\Users\msamson\Documents\MATLAB\test';
bits=8; % .lsm image format
speed=1; % radial averaging scheme
```

```
r_thresh=0.60; % thre shold for linear fitting of moment data
timeplotted=1:600; % how many frames are analyzed for second central moment
dispfig=0; %1 if want to display figures
fitpts=100; % # of points being fit if not using the rsq threshold
datach=1;
%--------------------------------------------------------------------------



warning('off','all')
% pixel size is 0.19 um
% time conversion is 0.0651s/frame

folderInfo=dir(fullfile(pn,'*.lsm'));

outFolder='C:\Users\abloom\Documents\Outimages';

folderInfo.name;

numFiles=length(folderInfo);

for imIndex=1:numFiles

    [imStack,imName]=LSMreader(pn,imIndex,bits);
```

```
    [~,~,sz]=size(imStack);
    % w=100;
    imStack_proc=imProcessor2(imStack);

    %build output name
    svnm=imName;
    for j=1:length(imName)
        if strcmp(imName(j),'.')==1
            svnm(j)='-'; %take out periods (these confuse the filetype)
        end
    end
    svnm=strcat(svnm,'.mat');
    f=fullfile(outFolder,svnm);
    save(f,'imStack_proc')
    imIndex

end

%%
% AUTHOR: Michael Samsom
% DATE: April 2013
% DESCRIPTION: This function reads .lsm files outputed from the Ziess
```

```
% confocal microscope. These are essentially a stack of TIFF images which are read in as
512X512Xnumberofsamples in 16 bit integer format

%-------------------------------------------------------------------------------------------------------------
---------------------------
function [imStack,imName] = LSMreader(pn,imIndex,bits)
% pn = 'C:\Users\Lab\Documents\Mike\Matlab Programs\KubitzDiff\test'; % this is the folder
containing LSM files
    % could be any path suchas /data/LSM/ or c:\data\LSM\
n=dir(fullfile(pn,'*.lsm'));


TT = Tiff(fullfile(pn,n(imIndex).name)); % open first LSM file
im = TT.read; % read image in current direcotyr

iminfo = imfinfo(fullfile(pn,n(imIndex).name)); % get meta data from LSM
subFileTypes = [iminfo.NewSubFileType]; % extract subfile types
actualImages = find(subFileTypes==0); % contains indices of TIFF-directories with 512x512
images

%loop to extract ALL images in file
imStack=uint16(zeros(512,512,600));
for i=1:length(actualImages)
```

```
    TT.setDirectory(actualImages(i));
    imStack(:,:,i) = TT.read;
end


switch bits
    case 8
        imStack=imStack*uint16(2^8);
    case 12
        imStack=imStack*uint16(2^4);
end

imName=n(imIndex).name;

 %multiplier because Ziess outputs 12-bit image
% implay(imStack) %plays movie of imStack

function filtnormimg=imProcessor2(img)

%%

check=0;
sz=size(img);
```

```
img_f=zeros(sz(1),sz(2),sz(3));
for ii=1:sz(3)
   img_f(:,:,ii)=ordfilt2(img(:,:,ii),5,ones(3,3));
end

grimg_f=mat2gray(img_f);

if check==1
   preInt=recoveryCurve(grimg_f,80,0);
end

% normalize images to one another using four corners
for j=1:sz(3)
   corners(j)= ( mean(mean(grimg_f(1:10,1:10,j))) + mean(mean(grimg_f(1:10,sz(2)-
9:sz(2),j)))...
       + mean(mean(grimg_f(sz(1)-9:sz(1),1:10,j))) + ...
       mean(mean(grimg_f(sz(1)-9:sz(1),sz(2)-9:sz(2),j))) )/4;
end

ref_int=max(corners);
% ref_int=mean(corners(1:5));
```

```
%  normalize using moving average window of 5
img_norm=zeros(sz(1),sz(2),sz(3));
scale_factor=mean(corners(1:5))/ref_int;
img_norm(:,:,1)=grimg_f(:,:,1)./scale_factor;
img_norm(:,:,2)=grimg_f(:,:,2)./scale_factor;

scale_factor=mean(corners(sz(3)-4:sz(3)))/ref_int;
img_norm(:,:,sz(3)-1)=grimg_f(:,:,sz(3)-1)./scale_factor;
img_norm(:,:,sz(3))=grimg_f(:,:,sz(3)-1)./scale_factor;

for j=3:sz(3)-2
   scale_factor=mean(corners(j-2:j+2))/ref_int;
   img_norm(:,:,j)=grimg_f(:,:,j)./scale_factor;
end

if check==1
   normInt=recoveryCurve(img_norm,80,0);
end

sz=size(img_norm);
% check normalization
for j=1:sz(3)
```

```
    corners_norm(j)= ( mean(mean(img_norm(1:10,1:10,j))) + mean(mean(img_norm(1:10,sz(2)-
9:sz(2),j)))...
        + mean(mean(img_norm(sz(1)-9:sz(1),1:10,j))) + ...
        mean(mean(img_norm(sz(1)-9:sz(1),sz(2)-9:sz(2),j))) )/4;
end

if check==1
    subplot(221),plot(preInt,'.')
    subplot(222),plot(corners,'.')
    subplot(223),plot(normInt,'.')
    subplot(224),plot(corners_norm,'.')
end

% Smooth pre-bleach image with 15X15 gauss kernel

preBleachDuration=20; %20 frames in this example may need to change
preBleachImage=zeros(512,512);

%  Calculates mean of all prebleach images
for ii=1:preBleachDuration
    preBleachImage=preBleachImage+img_norm(:,:,ii);
end
preBleachImage=preBleachImage./preBleachDuration;
```

```
avg=mean(mean(preBleachImage)); % this looked identical to filter method but is faster


% %  build gaussian lowpass filter
% hsize=[15 15]; %15 X 15 filter
% sigma=0.5; %standard deviation for gaussian filter
%
% H=fspecial('gaussian', hsize, sigma); %H is a filter structure
%
% filtPreIm=imfilter(preBleachImage,H,'replicate');


%  Divide all images by prebleach
% img_final_im=zeros(512,512,sz(3));
img_final_av=zeros(512,512,sz(3));


for ii=1:sz(3)
%     img_final_im(:,:,ii)=img_norm(:,:,ii)./filtPreIm;
    img_final_av(:,:,ii)=img_norm(:,:,ii)./avg;
end


% finalInt_im=recoveryCurve(img_final_im,80,0);


if check ==1
```

```
    finalInt_av=recoveryCurve(img_final_av,80,0);

%     subplot(221),plot(finalInt_im,'.')
%     subplot(222),plot(img_final_im(:,256,21),'.')
    subplot(121),plot(finalInt_av,'.')
    subplot(122),plot(img_final_av(:,256,21),'.')
end


filtnormimg=img_final_av;
```

A.2. D calculator (Analyze processed images to give a fitted D coefficient value presented in an excel file)

```
%%
%
% AUTHOR: Michael Samsom
% DATE: Feb 24, 2014 (version 2.0)
% DESCRIPTION: This is the main module of the FRAP analysis program.
```

```
clear all; close all; clc;


% VARIABLES-
%-------------------------------------------------------------------------
pn = uigetdir('C:\Users\abloom\Documents\processed and sorted images'); % get path from user
% pn='C:\Users\msamson\Documents\MATLAB\test';
xlsname='DiffusionSF69.xlsx';
bits=8; % .lsm image format
speed=1; % radial averaging scheme
r_thresh=0.60; % thre shold for linear fitting of moment data
timeplotted=1:600; % how many frames are analyzed for mhsecond central moment
dispfig=0; %1 if want to display figures
fitpts=100; % # of points being fit if not using the rsq threshold
datach=1;
%-------------------------------------------------------------------------



warning('off','all')
% pixel size is 0.19 um
% time conversion is 0.0651s/frame


folderInfo=dir(fullfile(pn,'*.mat'));
```

```
folderInfo.name;


numFiles=length(folderInfo);


out=zeros(numFiles,4);
for imIndex=1:numFiles
    fn=folderInfo(imIndex).name;
    [D,k,norm,rsq_norm]=allDiffFun(fn,pn);
    out(imIndex,1)=D.analytical;
    out(imIndex,2)=k;
    out(imIndex,3)=norm;
    out(imIndex,4)=rsq_norm;
    names{imIndex,1}=folderInfo(imIndex).name;
    imIndex
end


outstr={'D','k','Normslope','Image noise metric'};
rngstr1=strcat('A2:A',num2str(numFiles+1));
rngstr2=strcat('B2:E',num2str(numFiles+1));
xlswrite(xlsname,outstr,'B1:E1');
xlswrite(xlsname,names,rngstr1);
xlswrite(xlsname,out,rngstr2)
```

```
function [D,k,norm,rsq_norm]=allDiffFun(fn,pn)
% 1D diffusion model
%   DESCRIPTION:


%%%%%%%%%%%%%%%%%%%%%%%%%%%%%%%%%%%%%%%%%%%%%%
%%%%%%%%%%%%%%%%%%%%%%%%%%%%%
soumpfit=0;
analytfit=1;
momentfit=0;
taylorfit=0;
%%%%%%%%%%%%%%%%%%%%%%%%%%%%%%%%%%%%%%%%%%%%%%
%%%%%%%%%%%%%%%%%%%%%%%%%%%%%
% [pn,fn]=uigetfile('C:\Users\msamson\Documents\MATLAB\test-image-files\','*.mat');
imgin=load(strcat(pn,'\',fn));
img=imgin.imStack_proc; clear imgin;

% Convert proccessed images to data
im=mat2gray(img); % convert image to grayscale
im=imcomplement(im); % invert image
```

```
[l,w,d]=size(im);
% Check normalization
corner=zeros(1,d);
for j=1:d
   corner(j)=mean(mean(im(1:10,1:10,d)));
end
n_check=polyfit(1:d,corner,1);
yfit=polyval(n_check,1:d);
yresid=corner-yfit;
SSresid=sum(yresid.^2);
SStotal=(length(corner)-1*var(corner));
rsq_norm=1-SSresid/SStotal;
norm=n_check(1);



% Radial averaging
dummy=zeros(w,d,2);
dummy(:,:,1)=squeeze( im(:,256,:) );
dummy(:,:,2)=squeeze( im(256,:,:) );

%   full gaussians
dat=mean(dummy,3);
dat=dat(:,21:end); %eliminate
```

```
clear dummy

%   half gaussians
dummy(:,:,1)=flipud( dat(1:256,:));
dummy(:,:,2)=dat(257:end,:);
dathalf=mean(dummy,3);
clear dummy

dat2fit=dat(:,1:20:160); % for Taylor fit

% Get recovery curve (separate function)
recCurve=recoveryCurve(img,40,0);

F_inf=mean(recCurve(end-9:end));
F_0=recCurve(21);
Fo=mean(recCurve(1:20));
k=(F_inf-F_0)/(Fo-F_0);

Fi=mean(recCurve(:,20)); % prebleach intensity

recCurve=recCurve(21:end);
recCurve=(recCurve-recCurve(1))./(recCurve(end)-recCurve(1)); % fractional
recovery
```

```
% get initial conditions
%   Full gaussian for Taylor fit and w calculation
L=(l/2)*0.19;
X=linspace(-L,L,l);
Y=dat(:,1); Y=Y';

fitob=gausFit(X,Y);
coeffvals=coeffvalues(fitob);
n=512;
L=512*0.19;
x2=linspace(-L/2,L/2,n+1);
x=x2(1:n);
ic_full=coeffvals(1).*exp(-((x-coeffvals(2))./coeffvals(3)).^2);

% w_curve=ic_full(ic_full>exp(-2));

w_curve=Y(Y>(exp(-2)+min(Y)));

w=length(w_curve)*0.19;

w_half=w/2;
```

```
% %
% % fitting

%  Soumpasis fit method using recovery curve

t_char=5; % starting guess

options=optimset;

if soumpfit==1
    K=1;
    t_char_fit=fminsearch(@objSoump,t_char,options,recCurve,K);
    D_soump=w_half^2/(16*t_char);

    fitRec=soumpRecDiff(t_char_fit,K);
    hold all
    plot(recCurve,'.'),plot(fitRec);
    D.recovery=D_soump;
end




%%
%  Bessel solve method (from Carslaw & Jaeger, 1938)
%   this is a general solution to radial diffusion in a disk
if analytfit==1
```

```
    lambda=besselzero(0,50,1);  %zeros of besselj(0)
    D=15;                       %guess for D
    r=linspace(0,255,1000);     %build radius space for eqn solver
    r=r*0.19;                   %convert to um
    Y=interp1((0:255)*0.19,dathalf(:,1)',r);%get initial condition (this may
be better to do as average)
    fitobhalf=halfgaussfit(r,Y);
    cvals=coeffvalues(fitobhalf);
    a=cvals(1); b=cvals(2); c=cvals(3); %initial condition
    ichalf=a*exp(-r.^2/b)+c;
    tpts=10;
    width=length(ichalf(ichalf>(exp(-2)+ichalf(end))));

    %bessel oscillation buffer (width of ic must be small compared to R)
    rfit=linspace(0,255*15,1000*15);  %multiply by 15 to reduce BC atrifacts
    rfit=rfit*0.19;

    a=cvals(1); b=cvals(2); c=cvals(3); %initial condition with longer r
    ichalf2=a*exp(-rfit.^2/b)+c;

    count=1;
    for j=1:20:200
        OBS(:,count)=interp1((0:255)*0.19,dathalf(:,j),r);
        count=count+1;
    end

    D_an=fminsearch(@objAn,D,options,rfit,tpts,lambda,ichalf2,OBS,width);
```

```
    u_an=diffAnFun(D_an,rfit,tpts,lambda,ichalf2);
%
%     u_an2=u_an(:,1:1000);
%
%     figure
%     subplot(121)
%     plot(OBS)
%     SP=width; %your point goes here
%     yl=get(gca,'ylim');
%     line([SP SP], [yl(1) yl(2)])
%     title('DATA')
%
%     subplot(122)
%     plot(u_an2'),hold on%, plot(ichalf,'--r')
%     SP=width; %your point goes here
%     yl=get(gca,'ylim');
%     line([SP SP], [yl(1) yl(2)])
%     title('MODEL')
    D.analytical=D_an;
end


%%
%  Second central moment method
if momentfit==1
    k=KCalculator(im,w);
    [R,tind]=size(dathalf);
    rad=0:R-1;
    rad=rad*0.19;
```

```
    drad=rad(2)-rad(1);
    tind=200;
    incr=5;

    SSmom=zeros(1,ceil(tind/incr));
    count=1;
    for t=1:incr:tind
        SSmom(count)=trapz( ((rad.^2).*dathalf(:,t)'.*rad))*drad
/trapz(dathalf(:,t)'.*rad)*drad;
        count=count+1;
    end

    tvec=(0:length(SSmom)-1)*0.0651;
    p=polyfit(tvec,SSmom,1);
    yfit=polyval(p,tvec);
    yresid=SSmom-yfit;
    SSresid=sum(yresid.^2);
    SStotal=(length(SSmom)-1*var(SSmom));
    rsq=1-SSresid/SStotal;

    D_ss=p(1)/(k*4);
    D.moment=D_ss;
end
%%
%  Taylor expansion model (too slow with 2D case)

% OBS=dat2fit(l/2-r:l/2+r,:);
```

```
% result=fminsearch(@obj,D,options,coeffvals,OBS,l,r);
% model=oneDdiffdirfit(result,coeffvals(1),coeffvals(2),coeffvals(3));




% figure
% subplot(121)
% plot(dat2fit)
% ylim([0 1.1])
%
% subplot(122)
% plot(model')
% ylim([0 1.1])
% stri=strcat('D=',num2str(result));
% text(200,1,stri)


function [fitresult, gof] = gausFit(X, Y)
%CREATEFIT(X,Y)
[xData, yData] = prepareCurveData( X, Y );


% Set up fittype and options.
ft = fittype( 'gauss1' );
opts = fitoptions( ft );
opts.Display = 'Off';
opts.Lower = [-Inf -Inf 0];
opts.StartPoint = [0.927450980392157 246 87.9743453327971];
opts.Upper = [Inf Inf Inf];
```

```
% Fit model to data.
[fitresult, gof] = fit( xData, yData, ft, opts );


% % Plot fit with data.
% figure( 'Name', 'untitled fit 1' );
% h = plot( fitresult, xData, yData );
% legend( h, 'Y vs. X', 'untitled fit 1', 'Location', 'NorthEast' );
% % Label axes
% xlabel( 'X' );
% ylabel( 'Y' );
% grid on


function x=besselzero(n,k,kind)


%%%%%%%%%%%%%%%%%%%%%%%%%%%%%%%%%%%%%%%%%%%%%%%%%%%%%%%%%%%%%%%%%%%%%%%%%%%%%%%
%
% besselzero.m
%
% Find first k positive zeros of the Bessel function J(n,x) or Y(n,x)
% using Halley's method.
%
% Written by: Greg von Winckel - 01/25/05
% Contact: gregvw(at)chtm(dot)unm(dot)edu
%
%%%%%%%%%%%%%%%%%%%%%%%%%%%%%%%%%%%%%%%%%%%%%%%%%%%%%%%%%%%%%%%%%%%%%%%%%%%%%%%
```

```
k3=3*k;


x=zeros(k3,1);


for j=1:k3


    % Initial guess of zeros
    x0=1+sqrt(2)+(j-1)*pi+n+n^0.4;


    % Do Halley's method
    x(j)=findzero(n,x0,kind);


    if x(j)==inf
        error('Bad guess.');
    end


end


x=sort(x);
dx=[1;abs(diff(x))];
x=x(dx>1e-8);


x=x(1:k);


function x=findzero(n,x0,kind)
```

```
n1=n+1;     n2=n*n;

% Tolerance
tol=1e-12;

% Maximum number of times to iterate
MAXIT=100;

% Initial error
err=1;

iter=0;

while abs(err)>tol & iter<MAXIT

    switch kind
        case 1
            a=besselj(n,x0);
            b=besselj(n1,x0);
        case 2
            a=bessely(n,x0);
            b=bessely(n1,x0);
    end

    x02=x0*x0;
```

```
    err=2*a*x0*(n*a-b*x0)/(2*b*b*x02-a*b*x0*(4*n+1)+(n*n1+x02)*a*a);

    x=x0-err;
    x0=x;
    iter=iter+1;

end

if iter>MAXIT-1
    warning('Failed to converge to within tolerance. ',...
            'Try a different initial guess');
    x=inf;
end

function [fitresult, gof] = halfgaussfit(r, Y)
%CREATEFIT(R,Y)
%  Create a fit.
%
%  Data for 'radGauss' fit:
%      X Input : r
%      Y Output: Y
%  Output:
%      fitresult : a fit object representing the fit.
%      gof : structure with goodness-of fit info.
%
%  See also FIT, CFIT, SFIT.
```

```
%  Auto-generated by MATLAB on 05-Feb-2014 13:22:15



%% Fit: 'radGauss'.
[xData, yData] = prepareCurveData( r, Y );

% Set up fittype and options.
ft = fittype( 'a*exp(-x^2/b)+c', 'independent', 'x', 'dependent', 'y' );
opts = fitoptions( ft );
opts.Display = 'Off';
opts.Lower = [-Inf -Inf -Inf];
opts.StartPoint = [0.922483561088891 0.0110616532004999 0.176036416924799];
opts.Upper = [Inf Inf Inf];

% Fit model to data.
[fitresult, gof] = fit( xData, yData, ft, opts );

% % Plot fit with data.
% figure( 'Name', 'radGauss' );
% h = plot( fitresult, xData, yData );
% legend( h, 'Y vs. r', 'radGauss', 'Location', 'NorthEast' );
% % Label axes
% xlabel( 'r' );
% ylabel( 'Y' );
% grid on
```

```
function [ u ] = diffAnFun( D,r,tpts,lambda,ic )
%diffAnFun solves the 2D radial diffusion equation
%   Assumes radial symmetry, derivation adapted from Carslaw & Jaeger 1938
%       from the Proc London Math Soc
%   D is diffusion coefficient, lambda is the roots of the seroth bessel
%   function, ic must be same length as r
%   Functions sum limit is the same as length lambda

% r=linspace(0,R,1000);

if length(ic) ~= length(r)
    error('diffAnFun: ic not same length as r')
end

kmax=length(lambda);

dt=0.0651*20;
R=r(end);

% ic=(1)*exp(-(r.^2)/icparam.a);
dr=r(2)-r(1);

u=zeros(10,length(r));
for t=1:tpts
```

```
    for k=1:kmax
        J0=besselj(0,(lambda(k).*r)./R);
        J1=besselj(1,lambda(k));

        C=trapz(r.*J0.*ic )*dr/( (R^2/2)*J1^2 );

        u(t,:)=u(t,:)+( C*exp( (-lambda(k)^2*D*(((t-1)*dt)/R^2) ) ).*J0 );
    end

end



end
```

APPENDIX B: TIME SERIES OF IMAGES FROM FRAP EXPERIMENT

The following images are from an experiment analyzing the diffusion of 0.1mg/ml FITC-dextran in 1x PBS. Although the experiment consist of 600 images, for images 1-201, only 1 image for every 10 images will be displayed. For images 201-600, only 1 image for every 50 will be shown.

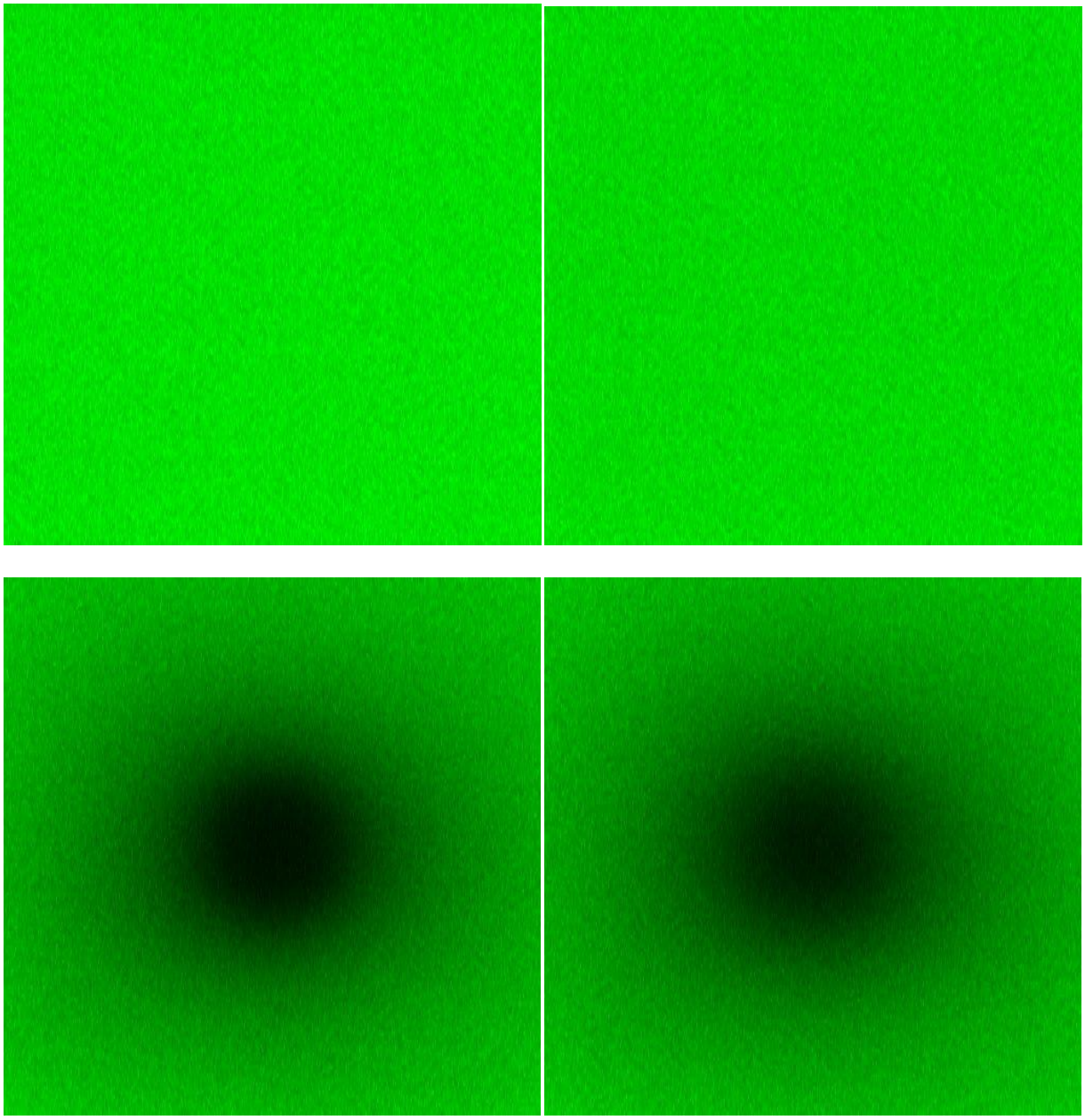

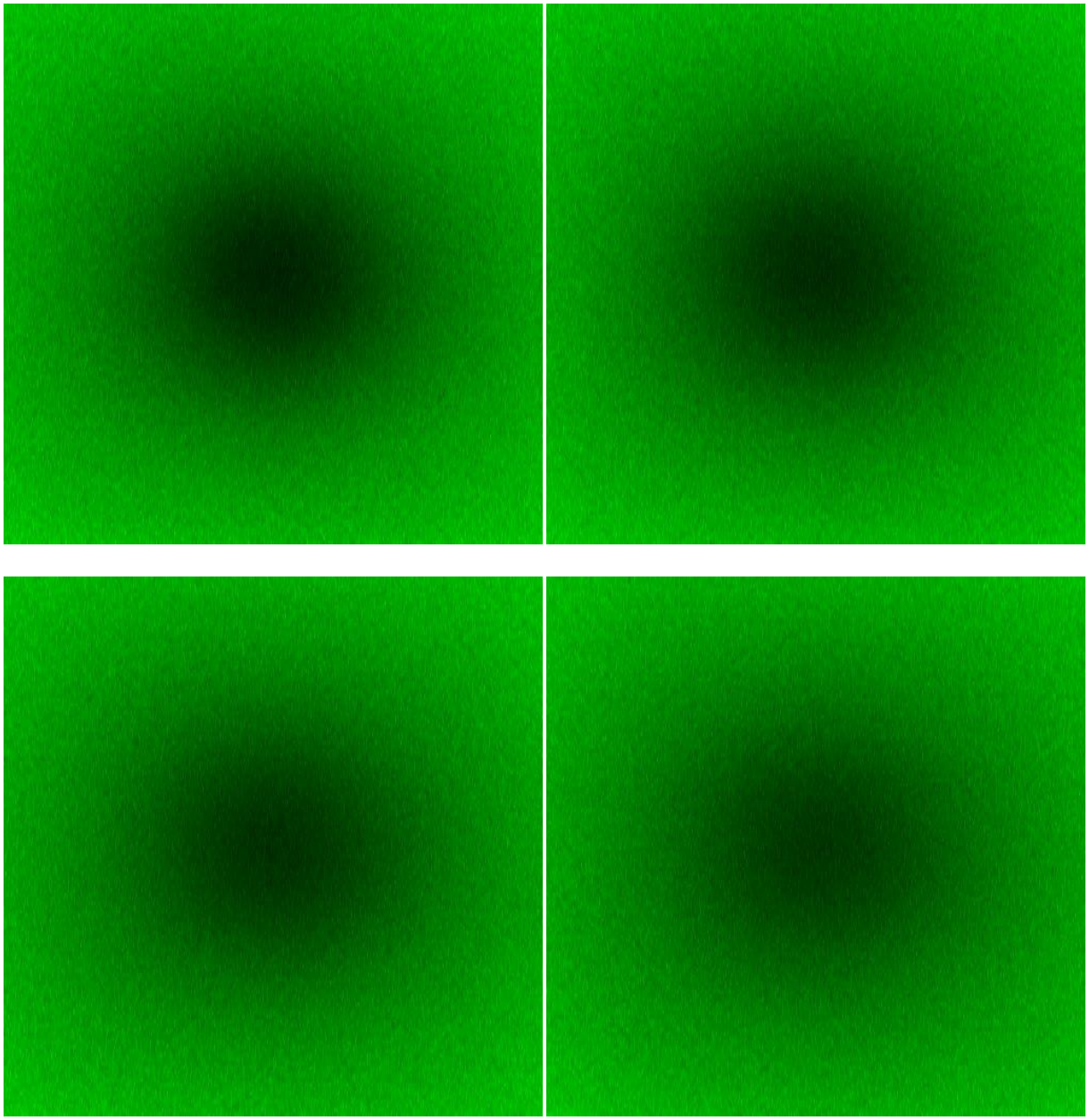

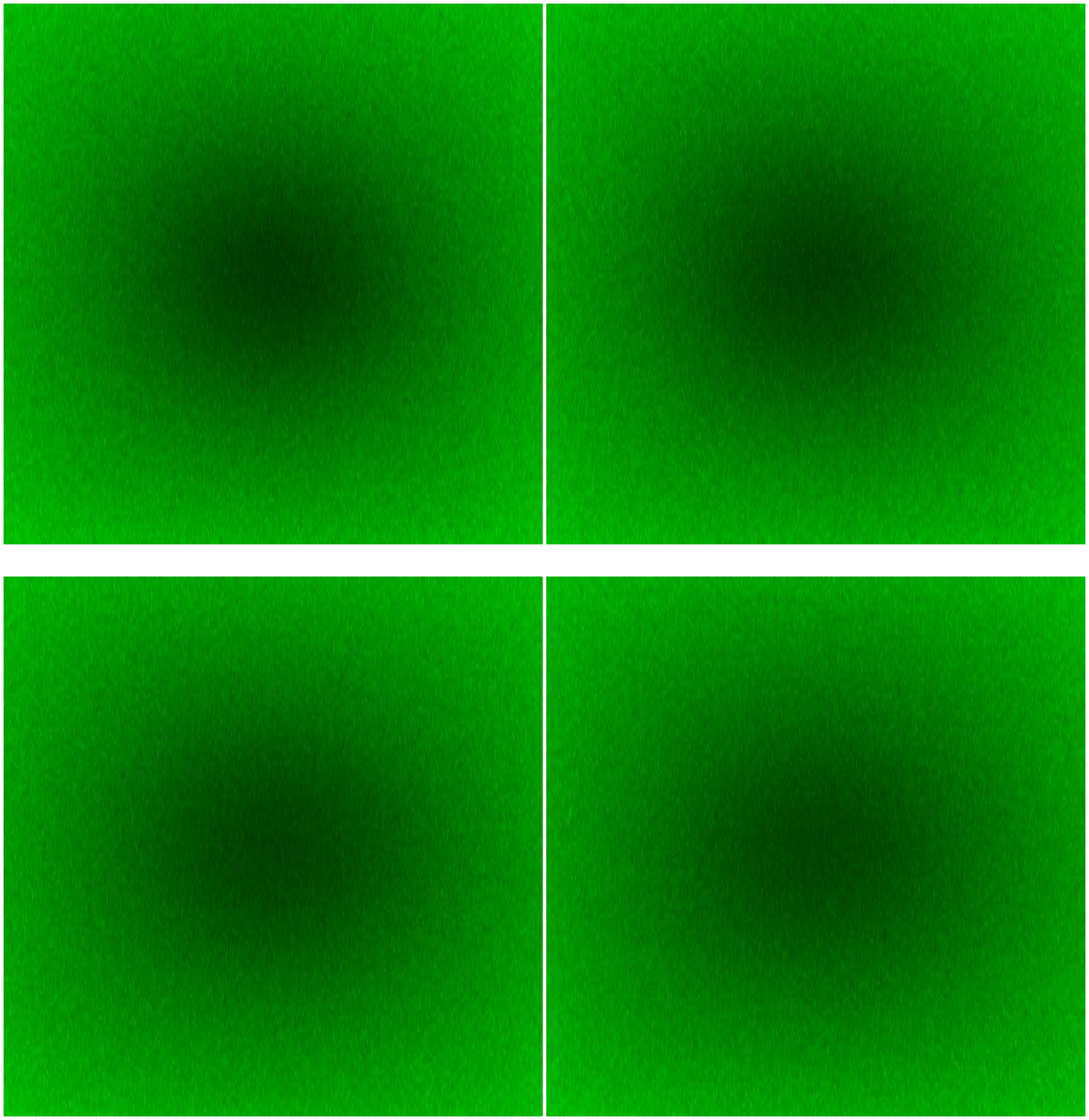

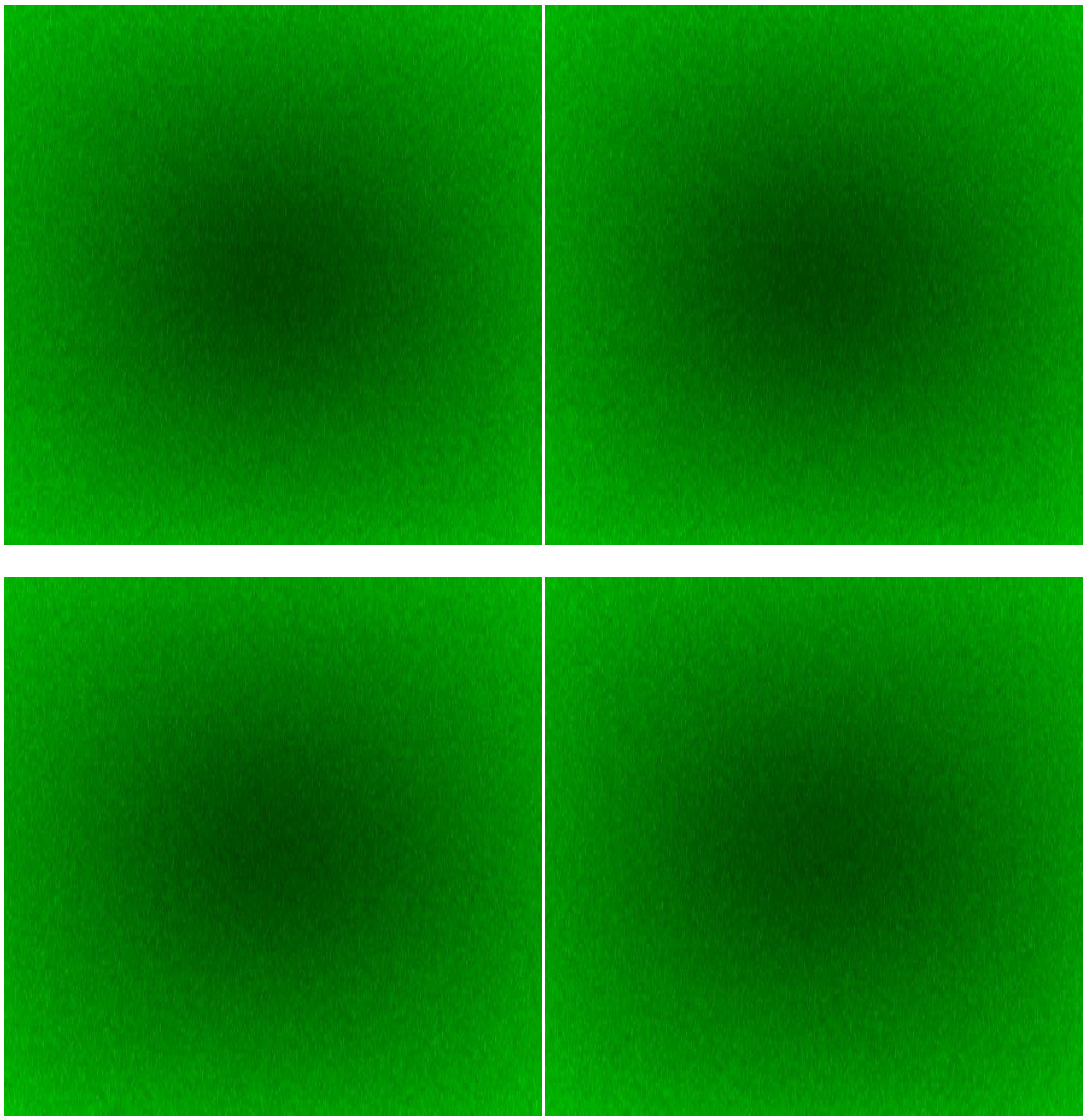

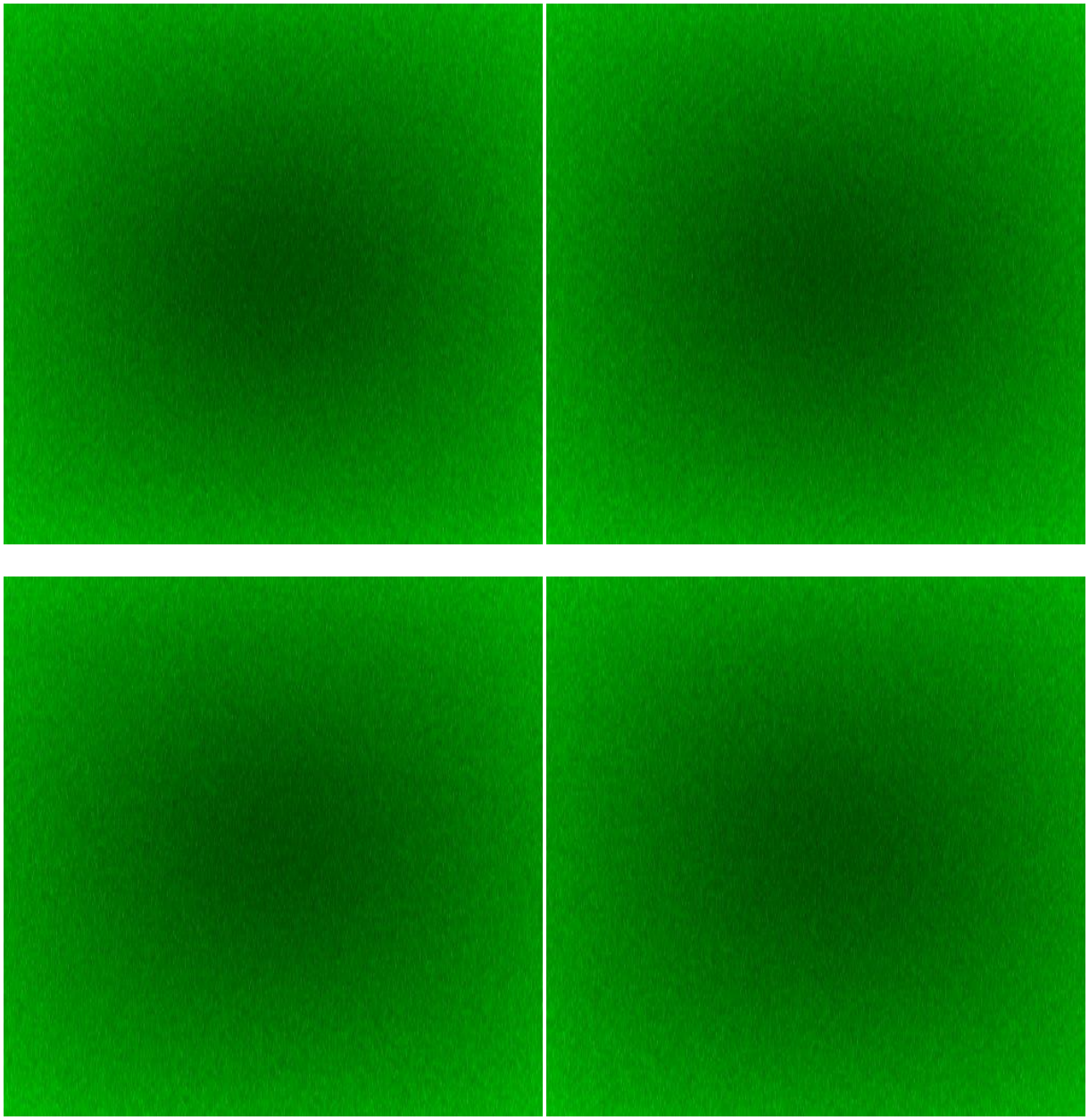

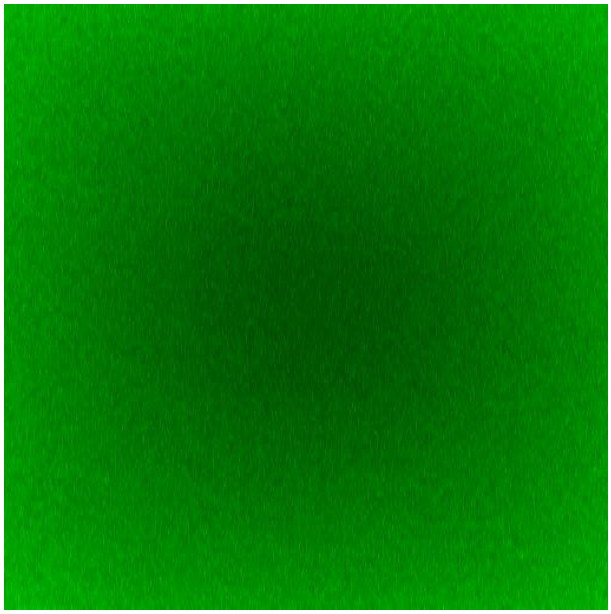

The next images represent images 251-600 in the time series.